Journal of Rock Mechanics and Geotechnical Engineering 15 (2023) 937–953

Contents lists available at ScienceDirect

Journal of Rock Mechanics and Geotechnical Engineering

journal homepage: www.jrmge.cn

Full Length Article

The role of soil in structure response of a building damaged by the 26 December 2018 earthquake in Italy

Angela Fiamingo, Melina Bosco, Maria Rossella Massimino*

Department of Civil Engineering and Architecture, University of Catania, Viale Andrea Doria 6, 95125, Catania, Italy

ARTICLE INFO

Article history:
Received 7 February 2022
Received in revised form
3 May 2022
Accepted 14 June 2022
Available online 16 July 2022

Keywords:
Local site response
Seismic risk
Reinforced concrete frame
Fully-coupled soil-structure system
Nonlinear dynamic analysis

ABSTRACT

Local soil conditions can significantly modify the seismic motion expected on the soil surface. In most cases, the indications concerning the influence of the underlying soil provided by the in-force European and Italian Building Codes underestimate the real seismic amplification effects. For this reason, numerical analyses of the local seismic response (LSR) have been encouraged to estimate the soil filtering effects. These analyses are generally performed in free-field conditions, ignoring the presence of superstructures and, therefore, the effects of dynamic soil-structure interaction (DSSI). Moreover, many studies on DSSI are characterised by a sophisticated modelling of the structure and an approximate modelling of the soil (using springs and dashpots at the foundation level); while others are characterised by a sophisticated modelling of the soil and an approximate modelling of the structure (considered as a simple linear elastic structure or a single degree of freedom system). This paper presents a set of finite element method (FEM) analyses on a fully-coupled soil-structure system for a reinforced concrete building located in Fleri (Catania, Italy). The building, designed for gravity loads only, was severely damaged during the 26 December 2018 earthquake. The soil was modelled considering an equivalent visco-elastic behaviour, while the structure was modelled assuming both the visco-elastic and visco-inelastic behaviours. The comparison made between the results of the FEM analyses and the observed damage is valuable.
© 2023 Institute of Rock and Soil Mechanics, Chinese Academy of Sciences. Production and hosting by Elsevier B.V. This is an open access article under the CC BY-NC-ND license (http://creativecommons.org/licenses/by-nc-nd/4.0/).

1. Introduction

It is well known that the main characteristics of seismic motion (amplitude, duration, and frequency content) can be modified by the local soil conditions through the geometry and physical properties of the soil layers. With this aim, Eurocode 8 Part 1 (EN 1998-1, 2004), as well as the in-force Italian Building Code (NTC, 2018), define a soil factor, *S*. For EN 1998-1 (2004), the soil factor depends on the soil category and the seismic hazard of the site, expressed by the surface-wave magnitude, M_S; on the other hand, for the NTC (2018), the soil factor (defined as $S = S_S S_T$) depends on the stratigraphic amplification factor, S_S, and the topographic amplification factor, S_T. In most cases, the soil factor, suggested by EN 1998-1 (2004) and NTC (2018), underestimates the real soil amplification. For this reason, in recent decades, the values of the soil factors reported in Building Design Codes have been modified for many times (Anastasiadis et al., 2001; Ansal et al., 2010, 2019; Lanzo et al., 2011; Ciancimino et al., 2018; Pagliaroli et al., 2020) and new ones have been proposed based on local seismic response (LSR) analyses (Pitilakis et al., 2012, 2019; Andreotti et al., 2018; Tropeano et al., 2018; Aimar et al., 2020; Paolucci et al., 2021).

Numerical analysis of LSR should be more greatly encouraged to estimate the soil filtering effects (Bardet et al., 2000; Kottke and Rathje, 2008; Ferraro et al., 2015; Hashash et al., 2020). Nevertheless, LSR analysis is generally performed in free-field conditions; thus, it does not consider the presence of superstructures and how this can modify the characteristics of seismic motion (FEMA P-2082-1, 2009). The damage caused by numerous, well-known earthquakes, i.e. Mexico City 1985, Loma Pietra 1989, Kobe 1995, Izmit 1999, L'Aquila 2009, Haiti 2010, and Norcia 2016, highlighted that the safeguarding of existing buildings and infrastructures and the planning of new ones must necessarily consider the effects of dynamic soil-structure interaction (DSSI) (Kausel, 2010). Several studies (Bielak, 1971; Veletsos and Meek, 1974; Luco, 1980) showed how the deformability of the soil influences the dynamic performance of the structure, determining both an extension of the vibration period and a damping increase: the seismic input induces

* Corresponding author.
E-mail address: maria.massimino@unict.it (M.R. Massimino).
Peer review under responsibility of Institute of Rock and Soil Mechanics, Chinese Academy of Sciences.

https://doi.org/10.1016/j.jrmge.2022.06.010
1674-7755 © 2023 Institute of Rock and Soil Mechanics, Chinese Academy of Sciences. Production and hosting by Elsevier B.V. This is an open access article under the CC BY-NC-ND license (http://creativecommons.org/licenses/by-nc-nd/4.0/).

energy that can be dissipated not only inside the structure but also inside the soil (geometric and hysteretic damping). Consequently, the DSSI effects would be beneficial. Nevertheless, depending on the soil and seismic input properties, maximum spectral ordinates have often been recorded at high periods (Mylonakis and Gazetas, 2000). In this case, the effects of the DSSI would be detrimental.

Preliminary analyses of DSSI are useful for estimating the seismic soil amplification or de-amplification and, consequently, for developing microzonation maps for a rational use of the territory. In this case, effortless approaches can be used due to the numerous structures to be examined (Rovithis et al., 2017; Abate et al., 2020). For a single structure or a reduced number of structures one next to the other, interaction effects can be carefully studied by in situ and laboratory tests (Paolucci et al., 2008; Pitilakis et al., 2008, 2021; Wang et al., 2011; Maugeri et al., 2012; Massimino and Biondi, 2015; Abate and Massimino, 2016; Massimino et al., 2019a; Amendola et al., 2021; Özcebe et al., 2021) or numerical analyses (Massimino et al., 2019b; Chaudhuri et al., 2020; Mercado et al., 2021).

DSSI effects can be determined by two approaches, i.e. "sub-structure" method and "direct" method. The first approach allows us to study the contribution of kinematic and inertial interactions (Mylonakis et al., 2006) separately. The direct method allows us to study the fully-coupled soil-foundation-structure system as a whole. The analyses are often performed numerically, considering more realistic initial and boundary conditions and material constitutive models (Wolf, 1985; Lysmer et al., 1999; Abate and Massimino, 2016; Abate et al., 2007, 2019). In the past, the direct method required a degree of computation that was unacceptable in the design of common structures; nevertheless nowadays, as Muir Wood wrote (2004) "*the power of the computers that are available to all geotechnical engineers has increased so much that it is quite reasonable to suggest that numerical analysis tools should be used much more as part of the routine of geotechnical design, incorporating the constitutive models of today and recognising the inadequacy of some of the simplifying assumptions that have been imposed in the past for reasons of calculational expediency*".

Many existing numerical analyses on soil-structure systems are characterised by a sophisticated modelling of the structure and an approximate modelling of the soil, using springs and dashpots at the foundation level (Jarernprasert et al., 2013; Elwardany et al., 2019). Other numerical analyses are characterised by a sophisticated modelling of the soil and an approximate modelling of the structure, considered as a simple linear elastic structure or a single degree of freedom system (Abate et al., 2008, 2010, 2016; Abate and Massimino, 2016; Pistolas et al., 2020). For all the above-mentioned reasons, it is advisable to study structures using the "direct" method, including the significant volume of soil interacting with the structures and an appropriate material model (e.g. inelastic behaviour). Furthermore, according to the best of the authors' knowledge, the conventional numerical analyses on soil-structure systems are performed on "ideal" structures, without the possibility of checking the real damage suffered.

This paper presents a set of numerical analyses, performed by the ADINA finite element code (Bathe, 1999), on a fully-coupled soil-structure system for a reinforced concrete building designed for gravity loads only. The building, located in Fleri (Catania, Italy), was severely damaged during the 26 December 2018 earthquake. For the building, two different behaviours are considered: linear elastic and nonlinear. For the soil, an equivalent visco-elastic behaviour is considered, and both rigid and deformable bedrock conditions are investigated. The case study presented examines the seismic performance of the building and the effects of the soil behaviour on the seismic system response. The results of the finite element method (FEM) analyses are compared with the real damage observed. Therefore, the present paper furnishes an interesting case study for the analysis of fully-coupled soil-structure systems.

2. Setting and earthquake data

Along the eastern flank of Mt. Etna, the largest volcano in Europe, many faults (belonging to the Timpe Fault System) cause frequent and diffuse seismic events with considerable damage despite their moderate magnitude (Azzaro, 2004; Azzaro et al., 2012; Alparone et al., 2013). The strongest earthquakes, reported in the seismic catalogue (CMTE Working Group, 2008), are characterised by a mean recurrence time of about 20 years, an epicentral intensity, according to the European Macroseismic Scale (EMS), of VIII $\leq I_0 \leq$ IX–X EMS (corresponding to a local magnitude (M_l) range of 4.3 $\leq M_l \leq$ 5, Azzaro et al. (2011; 2014)) and a shallow hypocentral depth (<5 km (Patanè et al., 2004; Alparone et al., 2015)). On 26 December 2018, an earthquake with M_w = 4.9 (M_l = 4.8, epicentral intensity of VIII EMS) located at a depth of less than 1 km struck the south-eastern flank of Mt. Etna. The epicentre (latitude 37.64°N and longitude 15.12°E, Fig. 1) was located along the Fiandaca fault, a 13 km-long late Quaternary fault in the Timpe Fault System (QUEST-WG, 2019). The earthquake produced severe damage (Civico et al., 2019; QUEST-WG, 2019), with Zafferana Etnea (550 m above sea level, Fig. 1) and its neighbouring village, Fleri, suffering the most.

In older reinforced concrete buildings, the seismic shaking induced the crushing and/or spalling of bricks in the partition and infill walls with, in some cases, in-plane or out-of-plane global collapse of the wall and cracks in the columns (Fig. 2a). Cracks occurred in many masonry buildings with filled, squared or hollow bricks and, in some cases, buildings suffered partial collapse (Fig. 2b) while many old, crumbling, rough stone buildings collapsed entirely. Religious buildings suffered severe damage, with widespread partial collapses. Part of the facade and apse collapsed in the church in Fleri, restored after the 1984 earthquake (Fig. 2c).

The accelerometer stations named as "SVN" and "EVRN", about 1 km apart, were the closest to the epicentre, respectively 4.5 km and 5.3 km away (Fig. 1b). The building investigated in this paper is in Fleri, 2.65 km from the epicentre, 4.04 km from the SVN station and 4.9 km from the EVRN station (Fig. 1b).

Acceleration time histories and elastic response spectra for the three components of the seismic motion (North-South "N-S", East-

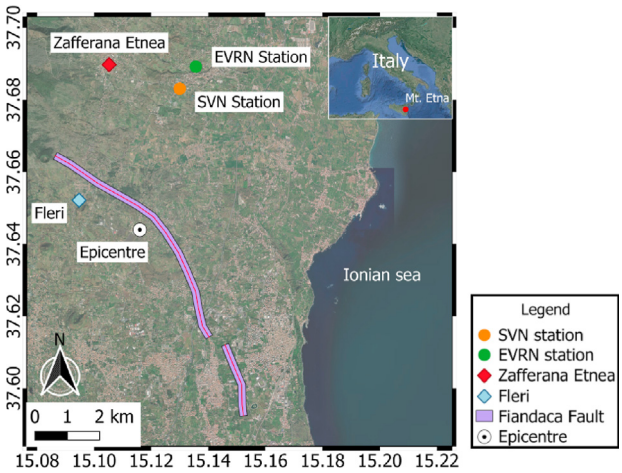

Fig. 1. Mt. Etna area and view of the Fiandaca Fault, the epicentre of the 26 December 2018 earthquake and the SVN and EVRN stations. The latitude and longitude are in degree.

Fig. 2. Damage caused by the 26 December 2018 earthquake in Fleri (Zafferana Etnea): (a) Breakage of partitions in reinforced concrete buildings; (b) Partial collapse of a masonry building; and (c) Details of the damage to the facade of the church in Fleri restored after the 1984 earthquake.

West "E-W", Vertical "V") recorded at each station are provided (Fig. 3). All the time histories are referred to soil type A, for which the weighted average value of the shear wave velocity ($V_{s,eq}$) up to the bedrock is greater than or equal to 800 m/s (Luzi et al., 2019) and each response spectrum is calculated for a damping ratio equal to 5%. In Fig. 3, the acceleration time histories of the EVRN station are translated to those of the SVN station given the mutual distance of the stations. The difference between the accelerations recorded at the two stations can be explained by the significant rock heterogeneity in the area. The E-W acceleration time histories recorded by both stations provide the greatest peaks: 0.56*g* and 0.3*g*, respectively, where *g* is the acceleration of gravity. Therefore, the numerical analyses (Section 4) will refer only to the E-W acceleration time histories recorded at the SVN station. The N-S, E-W and V response spectra were compared with those provided by the NTC (2018) for soil type A, for a return period of 475 years. The

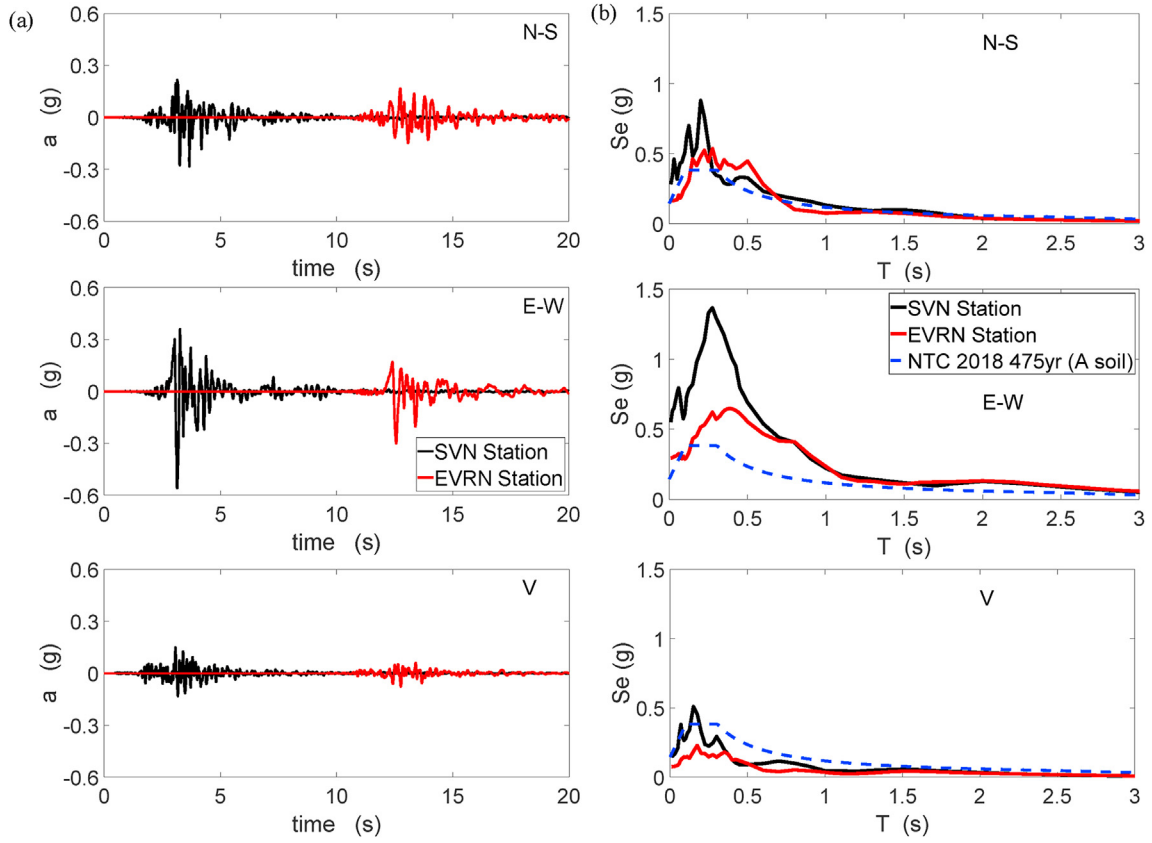

Fig. 3. Seismic motion: (a) Acceleration time histories recorded at the SVN station (black) and EVRN station (red); and (b) Elastic response spectra (5% damping) in comparison with the elastic response spectrum in the Italian Building Code (NTC, 2018) for a return period of 475 years.

spectral acceleration peaks for the SVN station are all above the elastic response spectrum provided by the NTC (2018), while, for the EVRN station, the peak occurs for a period greater than the one of the plateau of the NTC (2018) response spectrum. More specifically, the E-W response spectrum related to the SVN station shows the peak (1.4g) at $T = 0.26$ s, while for the EVRN station, the peak (0.58g) occurred at $T = 0.38$ s. Note that the period range of 0.2–0.4 s is critical for reinforced concrete or masonry structures having one-to-three elevations, such as the one investigated in this paper. For these structural categories, more significant structural damage is expected. These records confirm the high level of hazard on the eastern flank of Mt. Etna and that local seismicity deserves to be taken into due consideration as indicated by previous studies for the same return period, 475 years (Azzaro et al., 2008; 2013), with respect to the current NTC (2018) seismic zoning.

3. Case study

3.1. Soil profile

The dynamic soil characterization can be appropriately obtained by performing borehole investigations, such as cross-hole, down-hole and Marchetti seismic dilatometer tests. Alternatively, multi-channel analysis of surface waves (MASW) surveys can be performed. It is important to stress that the latter are non-intrusive and indirect investigations. MASW surveys, despite their limitations, are frequently performed when there is a lack of funds, as in the present case history, because they are fast, and low-cost tests. The building investigated is highlighted in red in Fig. 4a. MASW geophysical surveys were carried out 30 m from the building (see the yellow area in Fig. 4a), and given the reduced distance between the two, the stratigraphic profile obtained in this area (Fig. 4b) was used to characterise the soil underneath the building.

The MASW surveys were carried out to identify the shear wave velocity (V_s) along the soil profile, using 24 vertical geophones 1 m equidistant from each other. Recording of signals was performed by generating waves at two points placed at opposite ends of the geophones, with an offset of 2 m, for a total length of 27 m. The measurements were repeated three times to obtain more accurate information. The results are summarised in Fig. 5. From the profile of V_s–z, the weighted average value of the shear wave velocity up to the bedrock ($V_{s,eq}$) is equal to 365.7 m/s (Fig. 5). Thus, according to NTC (2018), the subsoil is of type B (characterized by a $V_{s,eq}$, between 360 m/s and 800 m/s) and the peak horizontal ground acceleration a_g concerning a probability of exceeding 10% in 50 years is equal to 0.225g. The stratigraphic amplification coefficient (S_S), equal to 1.16, is evaluated using the equation $S_S = 1.4-0.4F_0a_g/g$, where F_0 is the spectral amplification coefficient, and a_g is the design ground acceleration on soil type A (see Fig. 5 for the values of F_0 and a_g). As the site has a flat surface, the topographic category T1 was attributed and, consequently, the topographic amplification coefficient (S_T) is equal to 1. The mechanical properties of the soil are shown in Table 1. The shear modulus at small strain, G_{s0}, was obtained using Eq. (1) while the corresponding Young's modulus E_{s0} was obtained by Eq. (2).

$$G_{s0} = \rho_{s0}v_s^2 \tag{1}$$

$$E_{s0} = 2G_{s0}(1+\nu_s) \tag{2}$$

where ρ_s is the density and ν_s is the Poisson's ratio of the soil.

It is possible to modify the values of the soil shear wave velocity, shear modulus and the damping ratio according to Eurocode 8 Part 5 (EN 1998-5, 2004) to consider the soil nonlinearity in the absence of specific dynamic laboratory tests. The modified values, indicated with the symbols V_s^*, G_s^* and D_s^*, depend on the strain level, which in turn depends on value of a_gS. According to EN 1998-5 (2004), using the value of $a_gS = 0.26g$, reduction factors equal to 0.64 and 0.42 were estimated for G_{s0} and V_s, respectively, and $D_s^* = 8.5\%$ was established. In the numerical analyses (Section 4), V_s^*, G_s^* and D_s^* were used (Table 1).

3.2. Building

The typical Italian building investigated in this study is a reinforced concrete framed structure with three elevations designed according to the 1976 Italian Building Code (D.M., 1976) for gravity loads only. The layout of one typical floor and a structural section are shown in Fig. 6. The landings of the winding staircase are sustained by supporting beams belonging to the outer frame close to the street (Fig. 6b), which was damaged during the earthquake: cracking produced by shear forces occurred in the infills and columns close to the staircase (Fig. 7). The most significant damage occurred in the columns between the 2nd stair beam and the 2nd

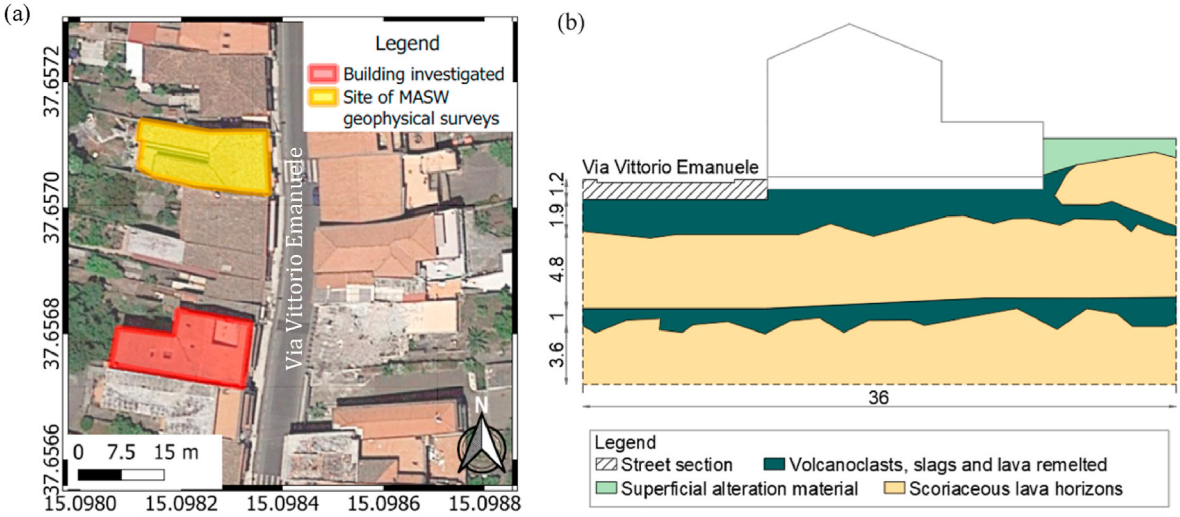

Fig. 4. In situ geotechnical tests: (a) Location of the building under study (red area) and the site for which the MASW surveys were carried out (yellow area) shown in Google Earth (2021), and (b) Soil profile at the site of MASW surveys (unit: m).

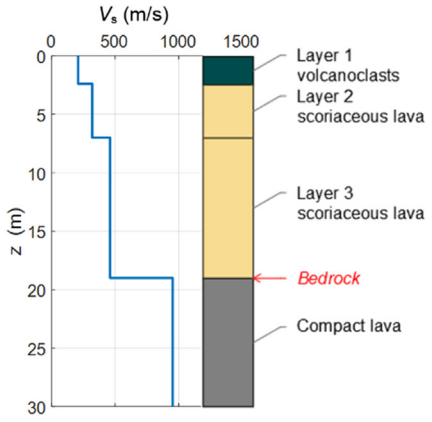

Seismic parameters according to NTC 2018	
Weighted average value of the shear wave velocity up to the bedrock	$V_{s,eq}$=365.7 m/s
Subsoil type	B
Maximum horizontal acceleration expected at the bedrock	a_g=0.225g
Spectral amplification coefficient	F_0= 2.644
Stratigraphic amplification coefficient	S_S=1.16
Topographic category	T1
Topographic amplification coefficient	S_T=1
Maximum horizontal acceleration expected at the soil surface (being $S = S_S S_T$)	$a_g S$=0.261g

Fig. 5. MASW survey results and evaluation of maximum acceleration expected at the soil surface according to NTC (2018).

floor. The present paper presents the results of the DSSI analyses for the frame highlighted by the red box in Fig. 6b.

A simulated design was carried out in line with the D.M. (1976) provisions to define beam and column cross-sections and reinforcements, based on the allowable stress method. In accordance with the Italian construction practice in the 1980s, the deck of the building under consideration is characterised by a top concrete slab with a thickness of 4 cm and reinforced concrete joists (with base $b_j = 8$ cm and height $h_j = 20$ cm) arranged along one direction. The distance between two consecutive joists is equal to 25 cm and was carried out assuming concrete with a characteristic cylinder strength f_{ck} equal to 20 MPa and a steel grade of FeB38k for rebars.

According to the D.M. (1976), these design assumptions lead to allowable stresses for concrete σ_c, and steel σ_s equal to 8.5 MPa and 215 MPa, respectively. The dimensions of the cross-sections of members were determined based on the available design drawings (Fig. 6): 30 cm × 60 cm for the superstructure beams; 50 cm × 70 cm for the foundation beam; 30 cm × 50 cm and 50 cm × 30 cm for the inside and outside columns on the first and second elevations, respectively; and 30 cm × 40 cm and 40 cm × 30 cm for the inside and outside columns on the third elevation, respectively (Fig. 8). The characteristic values of the permanent and variable loads (g_k and q_k) are equal to 4 kN/m^2 and 2 kN/m^2 for the deck, 6.1 kN/m^2 and 4 kN/m^2 for the stairs, and 4 kN/m^2 and 4 kN/m^2 for balcony, respectively. A characteristic permanent load equal to 6.83 kN/m is considered for infills.

The area of rebars was determined based on internal forces in beams and columns evaluated considering gravity loads only calculated as

$$A_s = \max\begin{cases} 0.003A_c \\ 0.006A_{c,req} \end{cases} \quad (3)$$

where A_c is the actual cross-sectional area of concrete of the column and $A_{c,req}$ is the minimum required cross-sectional area of the column calculated by

$$A_{c,req} = N / 0.7\sigma_c(1 + n\rho_l) \quad (4)$$

where N is the design axial force of the column evaluated according to the tributary area concept, n is the homogenisation coefficient for steel rebars (equal to 10), and ρ_l is the ratio of the longitudinal rebar area A_s to $A_{c,req}$ assumed equal to the minimum value required by the code (0.006).

Rebars with a diameter of 14 mm and 8 mm were used for longitudinal reinforcements and stirrups, respectively. According to the D.M. (1976), the spacing of stirrups and columns should not exceed the value 15 times the minimum diameter of longitudinal rebars. Thus, a spacing of 200 mm was defined. As concerns the beams, the minimum reinforcement ratio for the tension zone is equal to 0.0015. The required longitudinal reinforcement and stirrups for each span and each support at the typical floor were designed to sustain the maximum bending moments and shear forces determined assuming a simplified continuous beam. Rebars with a diameter of 14 mm or 20 mm were used for longitudinal reinforcements and of 8 mm for stirrups. The spacing of the stirrups was 100 mm at the ends of the beams, and 200 mm at midspan. A concrete cover of 2.5 cm was considered for all sections of the columns and beams. Fig. 8 shows the structural cross-sections of the columns and beams.

It should be noted that even if the building was not designed to sustain seismic action, the dimensions of the column cross-sections are much larger than those strictly required to sustain gravity loads. Because of this, the axial load ratio on the columns, strongly related to the ductility of the cross section, is moderate. Thus, even if it is expected to have poor inelastic capacity when compared to structures properly designed and detailed to sustain seismic action, the low axial load ratio improves the local ductility of these members slightly.

4. Numerical model

4.1. Fully-coupled soil-frame system (Models 1 and 2)

The ADINA code (Bathe, 1999) was used for all the FEM analyses both considering and ignoring the soil (Sections 4.1 and 4.2). Firstly,

Table 1
Main geotechnical properties of the soil.

Soil parameter	Value			
	Layer 1	Layer 2	Layer 3	Bedrock
γ_s (kN/m^3)	18	18	18	22
φ' (°)	33	33	33	40
c (kPa)	0	0	0	0
ν_s	0.3	0.3	0.3	0.45
h (m)	2.4	4.6	12	11
V_s (m/s)	209	320	460	953
G_{s0} (kPa)	78,625	184,320	380,880	1,998,060
E_{s0} (kPa)	204,427	479,232	990,288	5,594,567
D_{s0}	0.02	0.02	0.02	0.01
V_s^* (m/s)	135	207	460	953
G_s^* (kPa)	32,875	77,068	380,880	1,998,060
E_s^* (kPa)	85,475	200,378	990,288	5,594,567
D_s^*	0.085	0.085	0.085	0.01

Note: Shear wave velocity (V_s^*), elastic modulus (E_s^*), shear elastic modulus (G_s^*) and damping ratio (D_s^*) were modified according to EN 1998-5 (2004) to take into account soil nonlinearity; φ' is the friction angle; c is the cohesion; h is the soil layer thickness; D_{s0} is the soil damping ratio at small strain.

the soil-frame system was analysed considering two two-dimensional (2D) models, i.e. Models 1 and 2, as shown in Fig. 9, to consider the role of the soil in filtering the seismic waves and the possible DSSI effects. In both models, a visco-inelastic behaviour for the frame was assumed; for the soil elements, a visco-elastic equivalent constitutive model was used according to the "modified" parameters (see Table 1). Bedrock deformability was assigned as rigid for Model 1 and deformable for Model 2; in this last case, the bedrock deformability was modelled by dashpots (Lysmer and Kuhlemeyer, 1969). The beams and columns of the frame were modelled by elastic members with finite length plastic hinges at the two ends. The length of the hinges was set equal to the height of the member cross-section. Within the hinge region, the moment (M)–curvature (θ) curves were assigned, details of which will be discussed in Section 4.2. The beam horizontal displacements along the y-direction were linked by "constraint equations" that impose the same y-translation to reproduce an axial rigid diaphragm.

The soil mesh had a total depth of 19 m, according to the soil profile discussed in Section 3.1. The length was fixed equal to 100 m; a distance was obtained through an iterative procedure to reduce boundary effects as far as possible. Plane-strain four-node 2D-solid elements for the soil and two-node Hermitian beam elements for the structure were adopted, respectively. Along the lateral boundaries of the soil, constraint equations were defined to have the same y- and z-translations at an equal depth (see lines A-B and A'-B' in Fig. 9). The z-translation was fixed at the base of the dashpots, allowing only the y-translation (see line B-B' in Fig. 9). Contacts between the foundation and the soil were defined to simulate potential foundation sliding and uplifting. The foundation-soil friction angle (δ) was fixed equal to $2\varphi'/3$.

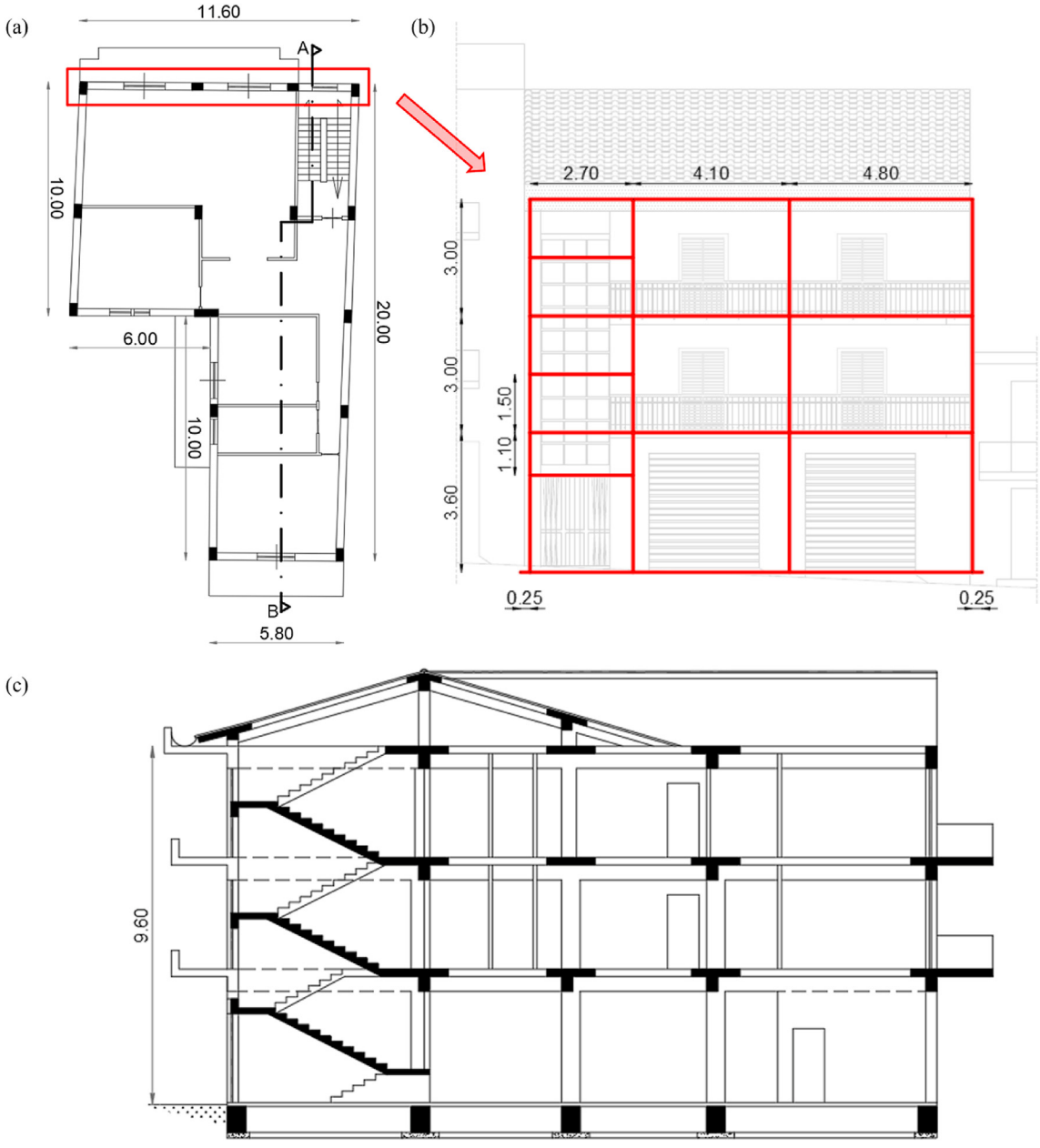

Fig. 6. The investigated building: (a) Typical floor plan, (b) View of the building from the street, and (c) Structural section AB (unit: m).

Fig. 7. Structural damage in the investigated building due to the 26 December 2018 earthquake: (a) Shear failure of the column (green shape) and breakage of infill panels (red shape), and (b) Subsequent demolition of infill panels.

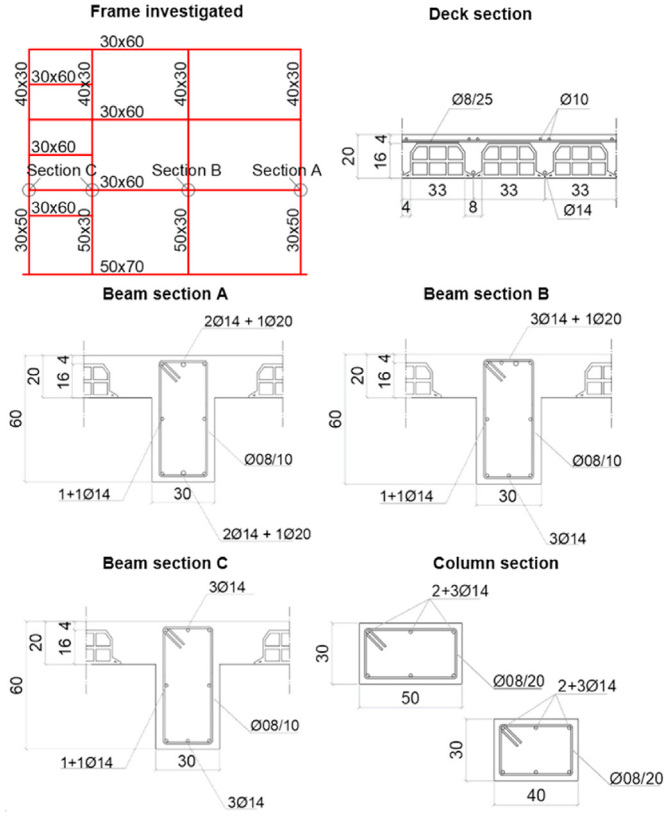

Fig. 8. Frame investigated and cross-sections adopted (dimensions of the sections in cm and rebars in mm). Ø is the diameter of the steel bars.

To obtain satisfactory numerical results, the maximum length of the mesh elements, h_{max}, must be computed according to the following equation (Lanzo and Silvestri, 1999):

$$h_{max} = V_s^* / (n f_{max}) \tag{5}$$

where f_{max} is the maximum significant frequency of the dynamic input (equal to 25 Hz), and n represents a value in the range of [6, 8]. Then, considering the smallest value of V_s^*, which is equal to 135 m/s (Layer 1, Table 1) the smallest value of h_{max} is equal to 0.675 m. The authors chose a length of 0.4 m for all the soil elements far from the frame, and 0.25 m for those near the frame.

The Rayleigh damping coefficients were estimated according to the following well-known equations (Chopra, 1995):

$$\alpha = 2D\omega_1\omega_2/(\omega_1 + \omega_2) \tag{6}$$

$$\beta = 2D/(\omega_1 + \omega_2) \tag{7}$$

where α is the first Rayleigh damping factor, β is the second Rayleigh damping factor, D is the damping ratio, ω_1 is the first natural angular frequency, and ω_2 is the second natural angular frequency.

For the soil, the first natural angular frequency was estimated by

$$\omega_1 = 2\pi V_{s,av}/(4H) \tag{8}$$

where H is the total thickness of the soil mesh and $V_{s,av}$ is the weighted average of the modified shear wave velocities of the whole soil mesh. The second frequency of the soil was assumed to be three times the first (Kwok et al., 2007). The Rayleigh damping coefficients for the structure were estimated according to Eqs. (6) and (7), where the fundamental frequencies were evaluated through the modal analysis of the inelastic fixed-base frame. The damping ratio D was assumed to be equal to D_s^* for the soil and equal to 5% for the frame. Table 2 shows the values obtained.

Distributed loads in the seismic design combination were applied to the beams. Furthermore, vertical forces were applied to the columns to consider gravity loads sustained by beams orthogonal to the frame. The mass of all the elements was also considered. The seismic input was set to the bedrock, using the E-W acceleration time histories recorded at the SVN station (see Section 2). Concerning the seismic input applied to the bedrock, for Model 1, it was directly applied to the base of the soil mesh, while for Model 2, it was applied to the dashpots located at the base of the soil mesh. Fig. 9 shows the free-field alignment and the four soil-structure alignments (DSSI) investigated in the following section.

4.2. Fixed-base frame (Models 3 and 4)

Secondly, the dynamic behaviour of the frame was analysed assuming the fixed-base condition and thus allowing only the y-translation (Fig. 10). Three FEM models, i.e. Models 3, 4 and 5, were developed.

The seismic motion applied to the foundation of Models 3 and 4 was the horizontal acceleration time history estimated in free-field

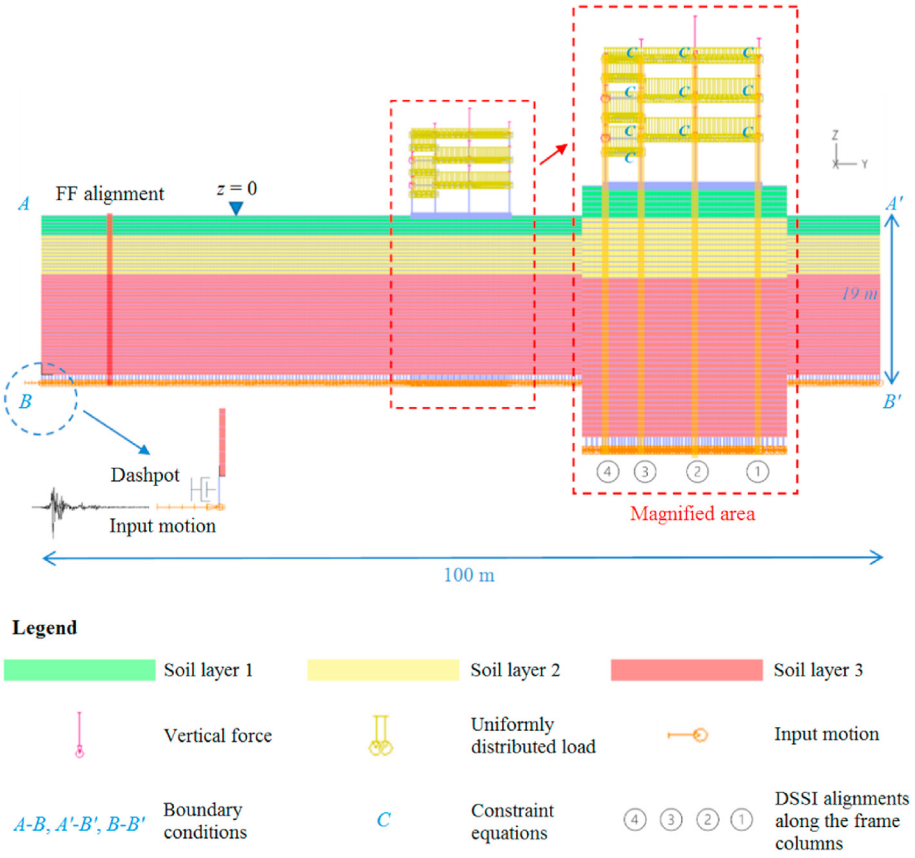

Fig. 9. FEM model of the entire soil-frame system (Model 1 and Model 2). FF is short for free-field.

Table 2
Evaluation of the Rayleigh damping coefficients α and β for the soil deposit and the visco-inelastic frame.

Parameter	Value	
	Soil	Frame
Frequency, f_1 (Hz)	3.52	1.37
Frequency, f_2 (Hz)	10.55	4
Rayleigh damping coefficient, α	2.82	0.64
Rayleigh damping coefficient, β	0.0019	0.0029

conditions in Model 2 (see Section 4.1). In addition, the SVN seismic motion, scaled to the value of a_gS according to NTC (2018), was applied to the foundation of Model 4, thus developing a fifth FEM model, i.e. Model 5. For Model 3, the beams and columns were modelled by elastic elements, while for Models 4 and 5, they were modelled by elastic members with finite length plastic hinges at the two ends. The length of the hinge was set equal to the height of the member cross-section, which was modelled using the M-θ curves preliminarily determined by the M-θ analysis carried out by the OpenSees (Mazzoni et al., 2006) computer program.

The concrete part of the cross-section was subdivided into fibres with a depth of 2 mm and a width equal to the width of the cross-section. The Mander constitutive law (Mander et al., 1988) defines this in OpenSees as 'Concrete04' uniaxial material, assigned to concrete fibres.

The values of the material parameters (elastic modulus E_c, mean compressive strength f_{cm}, concrete strain ε_{c0} at maximum strength, concrete strain ε_{cu} at crushing strength, and mean tensile strength f_{ctm}) are different for concrete fibres constituting the cover or the core of the cross-section (Table 3). Based on the values of strength directly obtained from cores extracted from about 400 buildings in Italy (Masi et al., 2014), an average compressive strength f_{cm} was assumed equal to 20 MPa for the cover region. The properties of the confined concrete were obtained by considering the confinement effectiveness factor for each cross-section, Eurocode 8 Part 3 (EN 1998-3, 2004). The value of compressive strength in the core region was only slightly larger than that in the cover region (ranging from 21.2 MPa to 24.3 MPa) because of low values of the confinement effectiveness factor.

For all the cross-sections analysed, a large concrete strain at crushing strength was assumed (5×10^{-2}) to avoid numerical instability. Single fibres enclosed in the cross-section were used to model rebars. An elasto-plastic constitutive law ('Steel01' uniaxial material in OpenSees) was assigned to the fibres. In line with the database provided in Simeone (2018), the average value of the yielding strength f_{ym} was set equal to 480 MPa. Fig. 11 shows the M-θ curves for the sections of the columns and beams. For columns, the curves were determined considering bending about either the strong or weak axis of the cross-section and for eight prefixed values of the axial force. Instead, for the beams, they were evaluated only about the strong axis for each cross-section.

5. Results of the FEM analyses

5.1. Results in free-field conditions

The LSR of the soil in free-field conditions was evaluated according to Models 1 and 2 along the free-field alignment (Fig. 9). Fig. 12a shows the acceleration time histories at the soil surface for

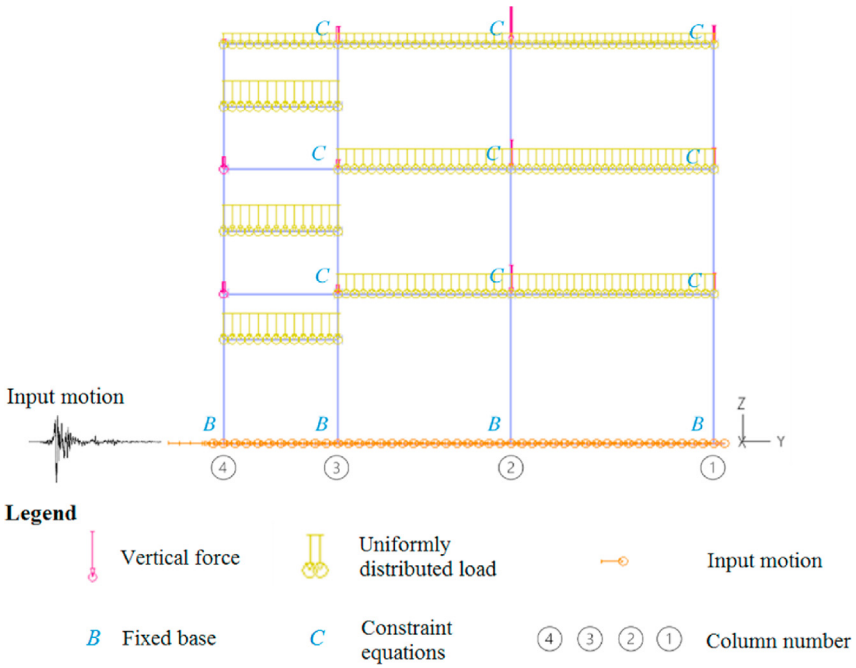

Fig. 10. FEM model of the fixed-base frame (Models 3 and 4).

Model 1 (rigid bedrock) and Model 2 (deformable bedrock) compared with that recorded at the SVN station. Fig. 12b shows the variation of the peak horizontal acceleration (*PHA*) with the soil depth (z). The *PHA*–z profiles obtained along the free-field alignment were also compared with the *PHA*–z profile obtained from one-dimensional (1D) site response analysis using the well-known 1D STRATA code (Kottke and Rathje, 2008). The comparison between 1D and 2D analyses is satisfying.

The rigid bedrock condition led to significant amplification of the seismic motion, with a peak value equal to 1.32g at the soil surface, corresponding to an amplification ratio $R_a = PHA_{surface}/PHA_{bedrock}$ equal to 2.43. On the other hand, the deformable bedrock condition led to a reduced increase of the motion amplitude equal to 0.86g (Fig. 12a and b) at the soil surface, corresponding to $R_a = 2.22$. Fig. 12b also displays the *PHA* expected at the bedrock and the soil surface according to the NTC (2018). In the present case, R_a had the same meaning as the stratigraphic amplification factor (S_s) reported in the NTC (2018), according to which the R_a expected at the soil surface ($S_s = 1.16$, see Fig. 5) is significantly lower than those obtained from the 2D analyses in other studies (Ferraro et al., 2015, 2018) for the same area. The different site seismicity, between that in the NTC (2018) and that recorded, underlines the need to identify the zones that are more exposed to seismic shaking (Azzaro et al., 2008; 2013), while the filtering role played by the soil between the bedrock and the above-ground structures must be a key aspect when evaluating their seismic response.

Fig. 13 shows the pseudo-acceleration response spectra ($S_e(T)$) referred to the soil surface in free-field conditions for a structure damping ratio equal to 5%. For Models 1 and 2, the maximum values of S_e were equal to 5.91g and 2.81g, respectively, and both reached at $T = 0.22$ s. As previously noted, in terms of the expected acceleration on the surface, the numerical results of Model 2 were more consistent with physical reality as the dynamic bedrock properties were considered. A pseudo-acceleration of 5.91g was out of scale. For both models, the elastic response spectra obtained from 1D and 2D modelling were also significantly higher than that given by the NTC (2018). It can be noted that the behaviour of the soil determined a significant increase in the pseudo-accelerations compared to the one recorded at the SVN station. No considerable translation of the frequencies at which the peaks themselves occurred was observed.

Fig. 14 demonstrates the amplification functions obtained considering the real soil stratigraphy (see 2D ADINA free-field analysis or 1D STRATA analysis) and a soil stratigraphy characterised by $V_{s,av}$, i.e. by a homogeneous soil (see 1D STRATA analysis, $V_{s,av}$).

The fundamental frequencies and the damping ratio of the soil were evaluated, employing the half-power bandwidth method for the latter. The first fundamental frequency of the soil was about 5 Hz, while the soil ratio damping was 8.5%. Considering $V_{s,av}$, i.e. a homogeneous soil, the amplification function obtained shows a first fundamental frequency equal to 3.48 Hz and a damping ratio equal to 8.5%. On the basis of these results, soil heterogeneity determined an increase in the amplitude of the amplification function and the first natural frequency, which is not taken into account by the NTC (2018) and Eurocode 8 Part 1 (EN 1998-1, 2004) that refer only to homogeneous soil, thus their proposed soil amplification factors are still questionable (Pitilakis et al., 2012, 2019; Andreotti et al., 2018; Tropeano et al., 2018; Aimar et al., 2020; Paolucci et al., 2021). As these analyses highlight, a careful geotechnical characterization of soil is a key aspect for evaluating the real seismic input at the soil surface. Local site response (LSR) analyses and detailed DSSI fully-coupled analyses should be always encouraged.

5.2. Results for the fixed-base frame

In this section, the results of the fixed-base frame (Models 3 and 4) are presented, highlighting the effect produced by its inelastic behaviour. These results will then be compared in Section 5.3, with those obtained for the soil-frame system to investigate DSSI effects.

Fig. 15a shows the *PHA* profiles along the fixed-base frame. The values are the same for each of its columns. At the top of the frame, the elastic and inelastic models provided a peak acceleration of

Table 3
Main concrete parameters for the investigated building.

Type	E_c (MPa)	f_{cm} (MPa)	ε_{c0}	ε_{cu}	f_{ctm} (MPa)
Unconfined concrete	22,360	20	2×10^{-3}	3.5×10^{-3}	1.57
Confined concrete 30 cm × 40 cm	23,380	21.9	2.93×10^{-3}	8×10^{-3}	1.57
Confined concrete 30 cm × 50 cm	23,027	21.2	2.61×10^{-3}	7.1×10^{-3}	1.57
Confined concrete beam	24,651	24.3	4.15×10^{-3}	1×10^{-2}	1.57

3.01*g* and 0.94*g*, respectively. This result confirms the importance of considering a nonlinear behaviour of the structure to obtain a more realistic estimate of its seismic behaviour. Indeed, an acceleration of 3.01*g* is incompatible with the real damage to the frame.

It is possible to evaluate the natural frequencies and the damping ratio of the frame compared to those in the modal analysis (Table 2), according to which, the first natural frequency and damping ratio are 1.37 Hz and 5%, respectively. In the amplification function shown in Fig. 15b (*FAS at the top*/*FAS at the foundation*), the first natural frequency is 1.33 Hz and the damping ratio is 20%. The latter produced a decrease in the amplitude of the seismic motion recorded on the frame itself (Fig. 15a) due to the nonlinear response of the structure. In all cases, there were no resonance effects, the first predominant frequency of the input applied at the foundation being equal to 4.44 Hz ($T = 0.22$ s, see Fig. 13).

Due to a lack of available structural data for old buildings, it is often necessary to execute a simulated design to reproduce the real behaviour of the structure. Uncertainty about the parameters used affects the characteristics assigned to the plastic hinges and, therefore, the numerical results. Thus, in situ tests should be performed to limit uncertainties. Despite these additional costs, unless fragile behaviour of members is expected to cause premature failure, a model that considers inelastic behaviour is recommended to obtain results that are closer to physical reality.

5.3. Results for the fully-coupled soil-frame system

In this section, the results obtained for Model 2 (deformable bedrock and an inelastic frame behaviour) are examined and compared with those obtained for Model 4.

Fig. 16 shows the *PHA* along the free-field alignment, the four alignments passing through the frame columns (Model 2) and the *PHA* expected at the soil surface according to the NTC (2018). The *PHA*–*z* profiles along the structure are quite different from those for the fixed base frame shown in Fig. 15a (Model 4). This result depends on the behaviour of the soil and foundation, which can modify the seismic input transmitted to the frame (Massimino et al., 2019b; Chaudhuri et al., 2020; Mercado et al., 2021). For the 4th DSSI alignment, the *PHA* is 0.99*g* at the soil-surface level and 0.85*g* at the foundation. Hence, the seismic motion was not fully transmitted from the soil to the foundation and this result

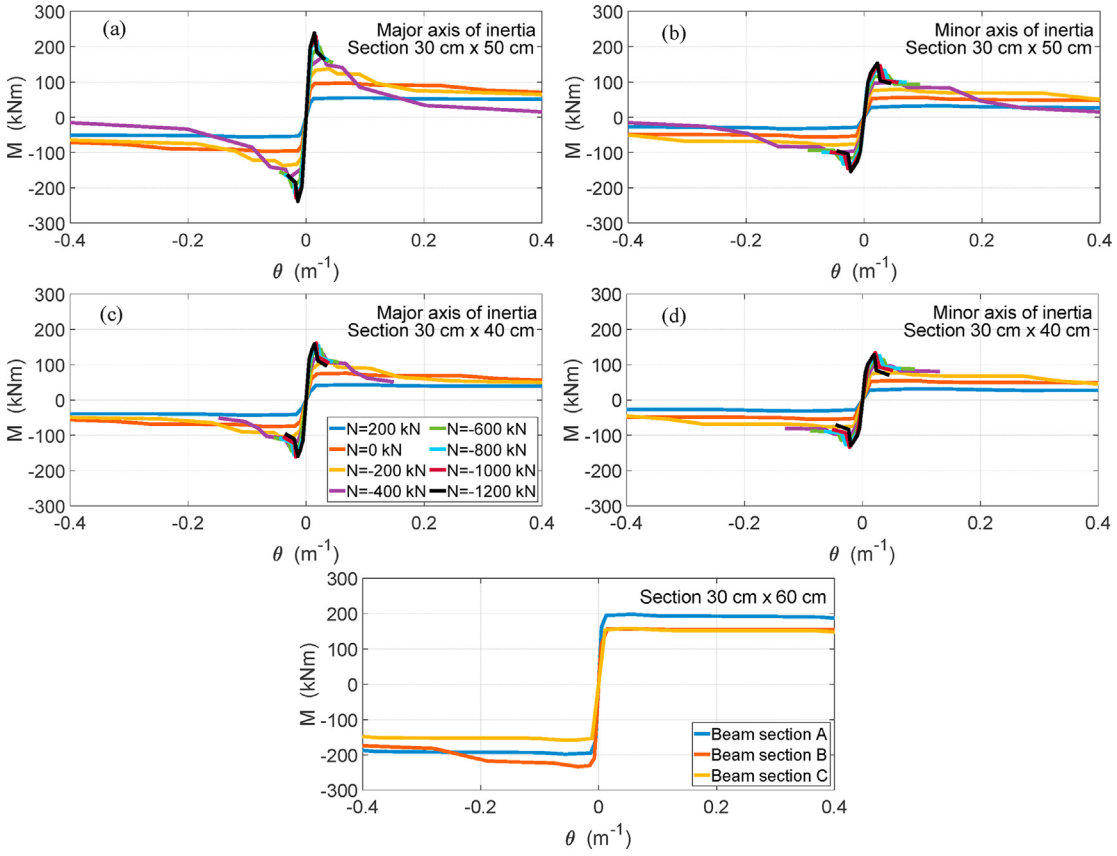

Fig. 11. Moment-curvature (M–θ) curves: (a)–(d) for the major and minor axes of 30 cm × 50 cm and 30 cm × 40 cm column sections, and (e) for the 30 cm × 60 cm beam section.

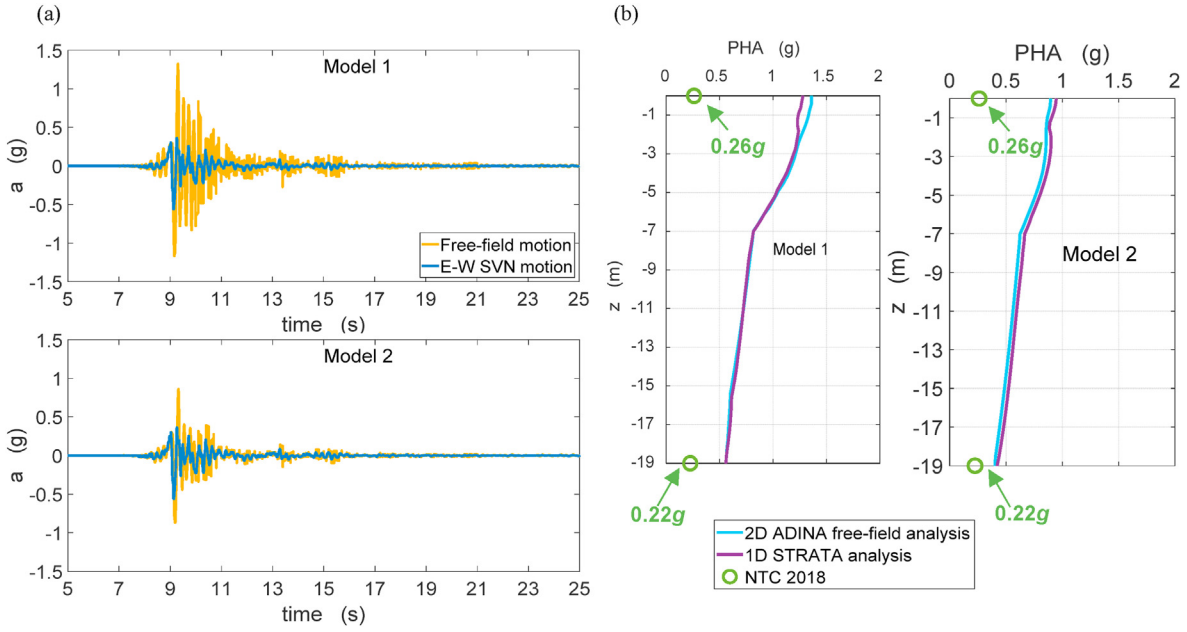

Fig. 12. Response of the soil in terms of acceleration: (a) Acceleration time histories obtained at the soil surface along the free-field alignment reported in Fig. 9, for Model 1 (rigid bedrock) and Model 2 (deformable bedrock) and E-W acceleration time history recorded at SVN station; and (b) Maximum accelerations along the vertical depth (z) of the soil deposit. The green circles report the acceleration expected at the bedrock and at the soil surface according to the in-force NTC (2018).

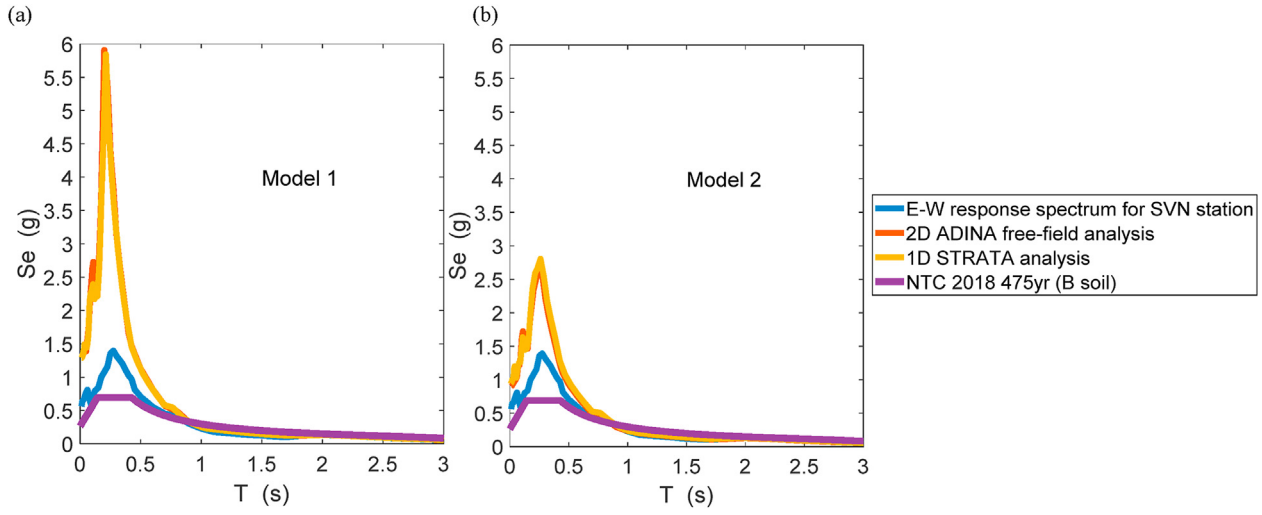

Fig. 13. Pseudo-acceleration response spectra in free-field conditions compared to the elastic response spectrum by the Italian Building Code (NTC, 2018) now in force: (a) for Model 1 (rigid bedrock) and (b) for Model 2 (deformable bedrock).

suggests that there was foundation–soil sliding. For the remaining alignments, the values of *PHA* at the soil surface and foundation are the same, approximately equal to 0.85*g*. In this case, the peak acceleration on the foundation is lower than that observed in free-field. This is a typical result for structures of this type which rest on medium stiffness soil (Karatzetzou and Pitilakis, 2017). The amplification ratios (R_a) are equal to 2.44, 2.11, 2.16 and 2.18 for the 4th, 3rd, 2nd and 1st alignments, respectively, compared to $R_a = 2.22$ for the free-field alignment.

Fig. 17 shows the time histories of y- and z-displacements (u, w) and soil-foundation relative horizontal (Δu) and vertical displacements (Δw) for points 4, 3, 2 and 1 in Model 2. The horizontal and vertical displacements for each column were evaluated at the foundation node and the soil node just below it. Evidence of foundation–soil sliding was observed only at point 4, as indicated by the slightly different y-displacement time

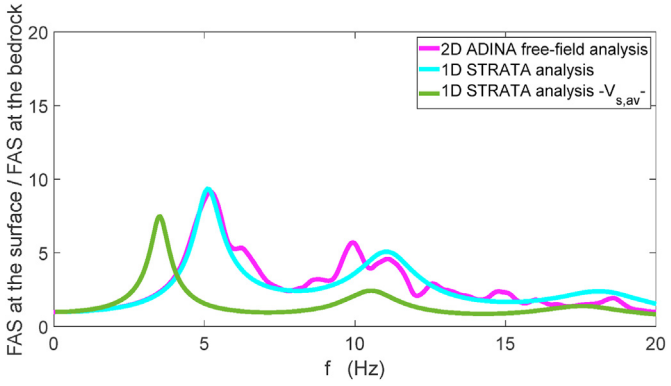

Fig. 14. Amplification function for 2D ADINA free-field analysis (magenta line) and 1D STRATA analysis for the case of heterogeneous (cyan line) and homogeneous soil (green line). f is the frequency.

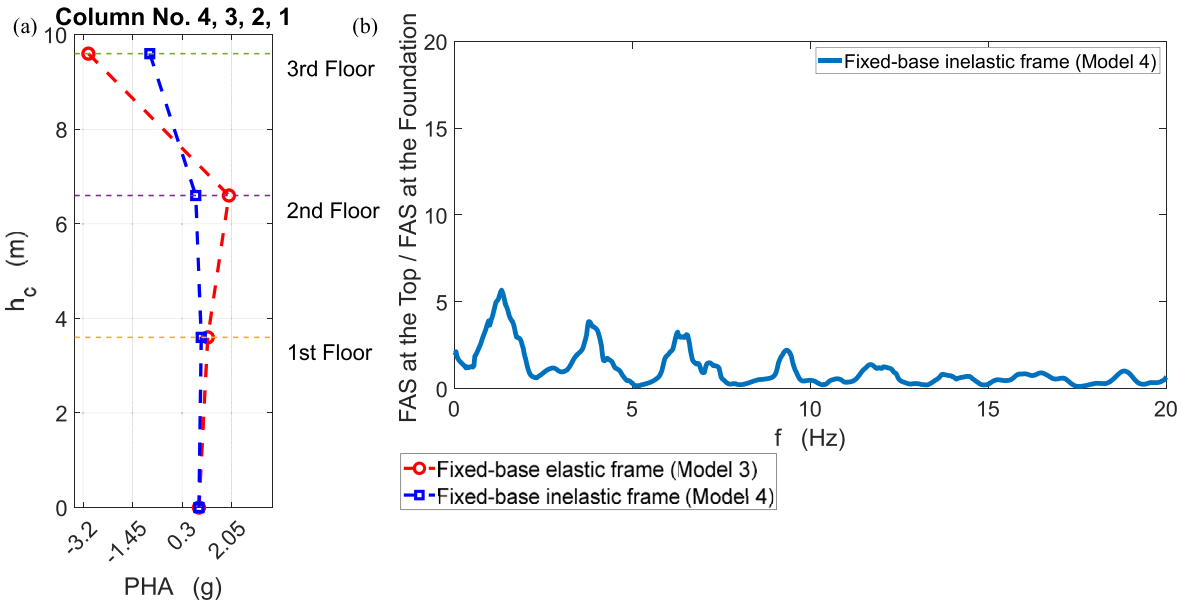

Fig. 15. Seismic response of the structure for Models 3 and 4: (a) Maximum acceleration along the fixed-base frame for the elastic frame (Model 3) and inelastic frame (Model 4), and (b) Amplification function for the inelastic frame (Model 4). FAS represents the Fourier amplitude spectrum and h_c represents the height of the reinforced concrete column.

histories. The vertical displacement time histories of the foundation node and the corresponding soil node were quite different. In particular, the foundation node at point 4 has uplifted by about 1 cm from the soil surface, as can be seen from the soil-foundation relative vertical displacement Δw. This caused a reduction of the stress at the corresponding column, as will be commented on later.

In Fig. 18a, it is possible to analyse the effects of DSSI on the frame observing the pseudo-acceleration response spectra for the horizontal component. The response spectrum was evaluated for the foundation and top nodes of the 4th column, comparing the results for Models 2 (soil-frame system) and 4 (fixed-base frame). It is useful to remember that the seismic motion applied to the foundation of Model 4 was the horizontal acceleration time history estimated in free-field conditions in Model 2 (see Sections 4.1 and 4.2). For the frame foundation, DSSI does not induce an increase in the spectral acceleration peak or a significant translation of the predominant period. At the same time, a slight decrease in the spectral acceleration peak was recorded at the frame top as compared to the fixed-base frame, suggesting that in this case the sliding and lifting effects of the foundation were modest.

Fig. 18b shows the amplification function of the soil, the whole soil-frame system, and the frame over the soil. It can be noted that the first frequency of the frame over the soil and soil-frame system are the same ($f \approx 1.11$ Hz). The latter frequency is lower than the first fundamental frequency of the same fixed-base frame, equal to 1.37 Hz ($T = 0.73$ s), obtained from the modal analysis. Depending on the characteristics of both the soil-frame system and the seismic motion, the fundamental soil frequencies decrease. The maximum spectral acceleration of the E-W response spectrum for the SVN station took place for a period of 0.225 s, which is far from the fundamental period of the soil–frame system, thus no resonance

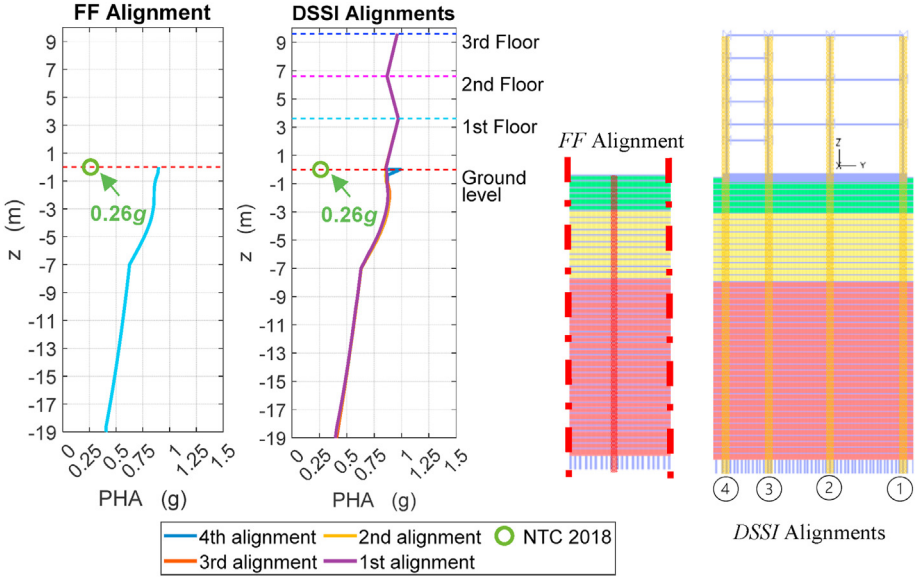

Fig. 16. Maximum acceleration profiles along the soil in free-field condition (FF alignment) and under each column's frame (DSSI alignments) and along each column's frame for Model 2. The green circle represents the expected acceleration according to the in-force NTC (2018).

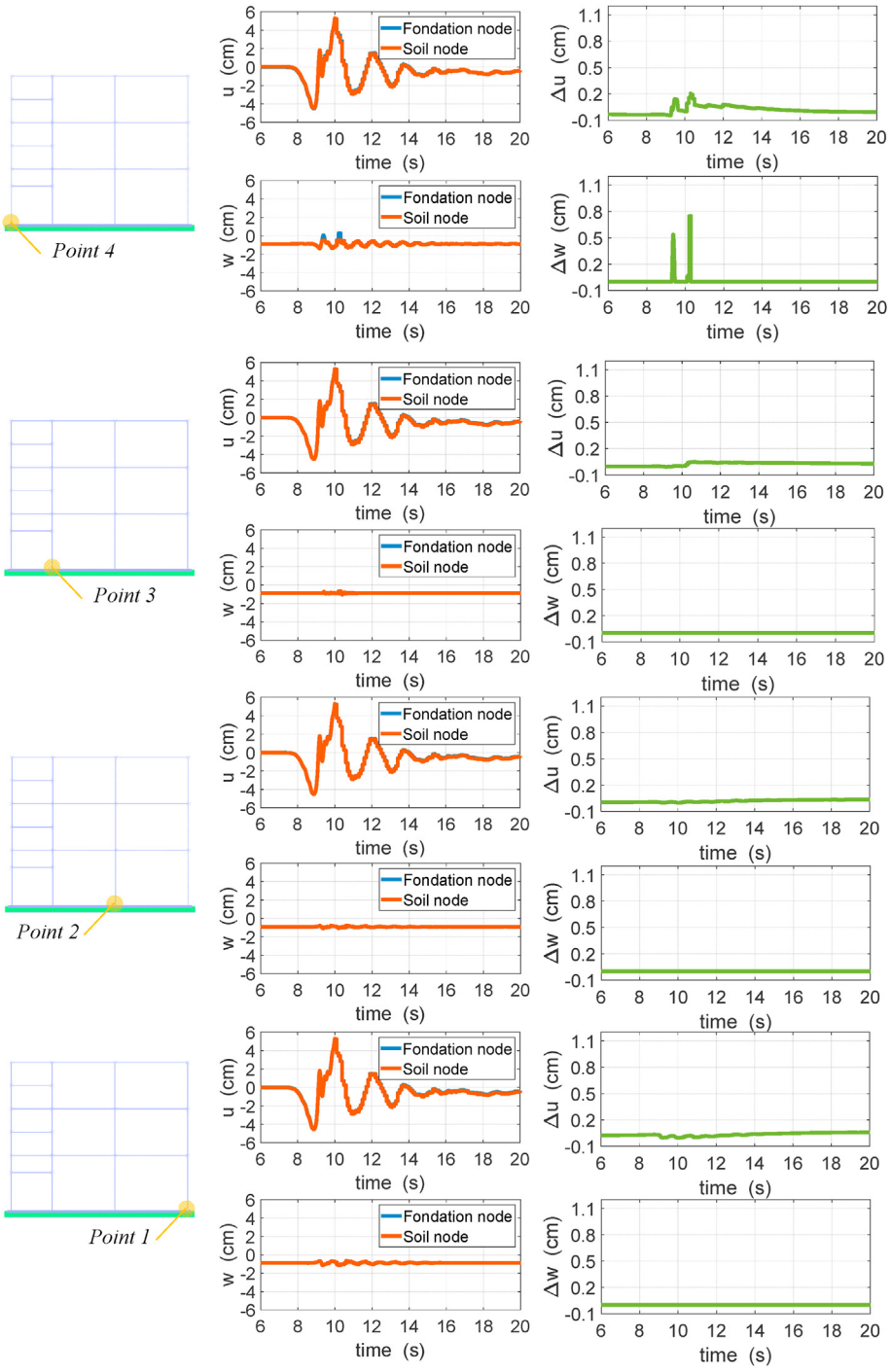

Fig. 17. Time histories of y-displacement (u), z-displacement (w), soil-foundation relative horizontal displacements (Δu), and soil-foundation relative vertical displacements (Δw) for points 4, 3, 2 and 1 (Model 2).

phenomena occurred. Employing the half-power bandwidth method, the frame placed on the soil showed a damping ratio lower than the fixed-base frame (13% versus 20%).

5.4. Comparison between the FEM results and the actual damage to the frame

Finally, the numerical results obtained for Models 2, 4 and 5 are compared with the actual damage to the frame in terms of the dimensionless ratio V_{max}/V_{Rd}, being V_{max} the maximum shear force and V_{Rd} the resistant shear force for the four frame columns, evaluated for each floor and the staircase beams (Fig. 19).

V_{Rd} was calculated as the minimum between the shear force which can be sustained by the yielding shear reinforcement and the shear force which can be supported by the member, limited by crushing the compression struts. The average resistance of concrete (f_{cm}) and steel (f_{ym}) are divided by the relevant partial safety factors required by Eurocode 8 Part 3 (EN 1998-3, 2004). No tests on the effective resistance of materials were available. Due to the uncertainty of the resistance parameters, the occurrence of shear failure was established when $V_{max}/V_{Rd} \geq 0.9$.

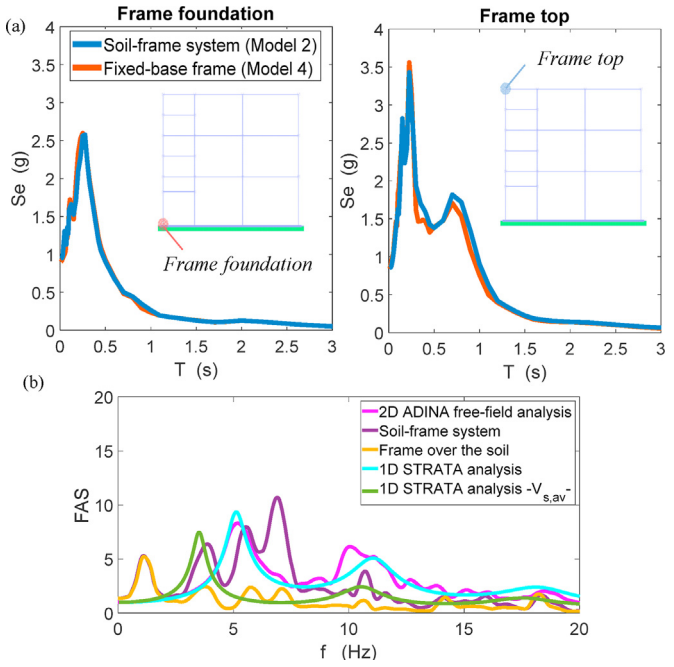

Fig. 18. Seismic response of the soil and the structure: (a) Pseudo-acceleration response spectra for inelastic fixed-base frame and the entire soil-frame system (data for column 4), and (b) Acceleration transfer function.

Fig. 19 indicates the occurrence of shear failure ($V_{max}/V_{Rd} \geq 0.9$) only for the 3rd column, being the one damaged by the seismic event. Model 2 provides values near $V_{max}/V_{Rd} \geq 0.9$ in the 3rd column close to the 2nd and 3rd stair beams and Model 4 shows $V_{max}/V_{Rd} \geq 0.9$. The V_{max}/V_{Rd} versus h furnished by Model 2 agrees with the most significant damage that occurred in the columns between the 2nd stair beam and the 2nd floor during the earthquake. Both models furnish large shear forces in the columns close to the 2nd and 3rd stair beams; but in Model 4, the damage to the 2nd floor is not markedly highlighted.

Except for columns 4 and 3, for which sliding and uplifting soil-foundation phenomena were observed in Model 4, for columns 2 and 1, the results of Models 2 and 4 are similar. Nevertheless, overall Model 2 showed results more consistent with the real damage.

Model 5 shows much smaller values of V_{max}/V_{Rd} than those corresponding to the shear failure for all the columns. A comparison between Models 4 and 5 clearly shows that the soil contribution is not captured by the stratigraphic amplification coefficient reported in the NTC (2018). The conventional analysis in line with the NTC (2018) (Model 5) would not have shown any damage. The results confirm that earthquake damage is not necessarily a "physical" process for such buildings and can be captured only by considering the local soil amplification phenomena.

6. Conclusions

This paper presents a set of numerical analyses on a fully-coupled soil-structure system for a reinforced concrete building, located in Fleri (Catania, Italy) in the eastern area of Mt. Etna. The building, designed for gravity loads only, was severely damaged during the 26 December 2018 earthquake. Italy has a wealth of structures designed without seismic criteria, thus it is a priority to investigate the seismic behaviour of these buildings and highlight the fundamental role of the soil. The aim of this paper was to examine the seismic performance of the building and the effects of the soil behaviour on the structure response, including the effects of the bedrock deformability and the inelastic structure behaviour. The FEM analyses performed allow us to underline the following aspects:

(1) The importance of seismic hazard, especially for built-up areas. During the 26 December 2018 earthquake, the PHA recorded on soil type A by the stations (SVN and EVRN)

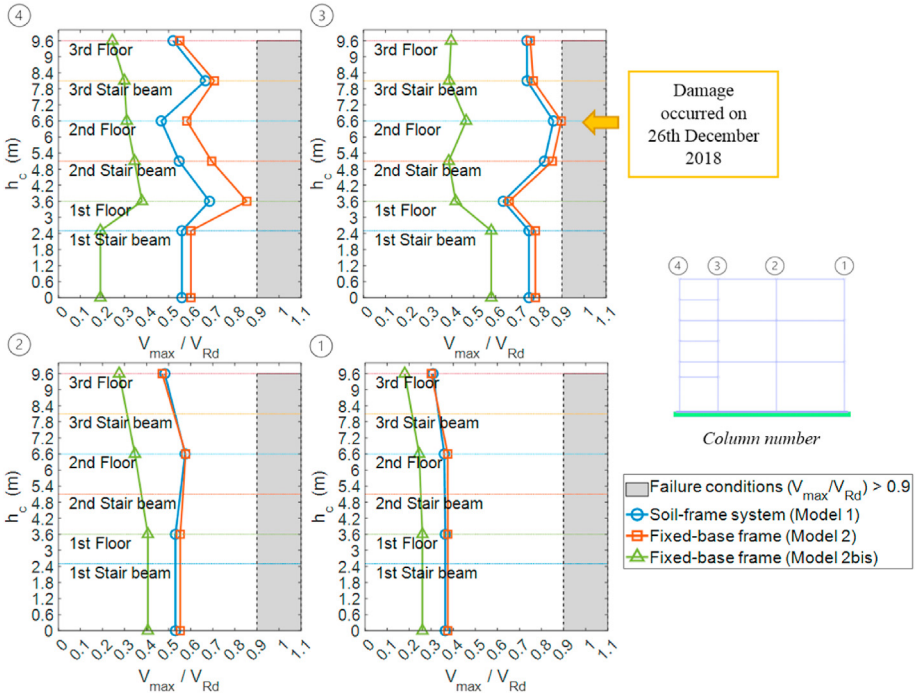

Fig. 19. Dimensionless ratio V_{max}/V_{Rd} along the frame columns.

nearest to the building investigated was 0.56*g* and 0.3*g*, respectively. These records confirm the high level of hazard in the eastern part of Mt. Etna, characterised by earthquakes of low recurrence time, high epicentral intensity, and shallow hypocentral depths (Patanè et al., 2004; Azzaro et al., 2011, 2014; Alparone et al., 2015). This highlights the important role of hazard maps to indicate the zones that are more exposed to seismic shaking, in order to establish retrofit actions for urban areas. Nevertheless, the current seismic zoning (NTC, 2018) does not fully acknowledge the real hazard level of this area. For the same soil condition, the NTC (2018) furnishes a design ground acceleration of 0.225*g*.

(2) It is necessary to consider the real stratigraphy of the soil and its geotechnical properties. The amplification and de-amplification of the seismic motion due to soil filtering phenomena, together with the site seismicity, are key aspects when evaluating the seismic response of structures. In this case study, the amplification ratio expected at the soil surface according to the NTC (2018) ($S_S = 1.16$) was significantly lower than those obtained from the 2D analyses ($R_a = 2.43$ for rigid bedrock and 2.22 for deformable bedrock). According to other studies (Ferraro et al., 2015, 2018) for the same area, the stratigraphic amplification coefficients reported in the NTC (2018) were not completely appropriate, suggesting the need for a possible review. LSR analysis should be more greatly encouraged, also in routine design.

(3) The importance of reliable numerical modelling. The numerical modelling of the soil cannot ignore the dynamic properties of the bedrock. The modelling of the structure cannot be performed in the elastic range, especially for severe seismic events. Results that consider both the bedrock deformability and the inelastic behaviour of the structure are closer to the experimental reality in terms of pseudo-acceleration response spectra and maximum acceleration along each floor. Accurate data of the soil conditions and parameters, as well as reliable and well accepted M-θ curves for structural elements can also be obtained with a reasonable degree of computation and economic outlay. Nowadays, FEM analyses of fully-coupled soil-structure systems must also be encouraged for all buildings thanks to the tremendous development of calculation power. In this case, the DSSI analyses allowed us to evaluate modest uplifting and sliding between the foundation and the soil. The peak acceleration on the foundation deserves particular attention as it could be different to that in free-field conditions. For the type of structure and medium stiffness soil profiles under analysis, the peak acceleration at foundation level was higher than that observed in free-field.

(4) The comparison between the results of the FEM analyses and the real damage observed confirm that the damage after an earthquake is not necessarily a "physical" process for vulnerable buildings. Even though the building under investigation in these analyses is a non-seismically designed structure, it was demonstrated that the damage observed could be captured only by a careful analysis of the local soil amplification phenomena. The building under investigation, subjected to the SVN seismic motion on 26 December 2018 scaled to the value of a_gS according to the NTC (2018), would not have suffered damage.

(5) The present paper furnishes an interesting approach for studying fully-coupled soil-structure systems, for the retrofitting of existing structures and the design of new ones, with a reasonable amount of computation, comparing the results of the FEM analyses of the building with the real damage observed, including soil filtering phenomena and inelastic structure behaviour.

Declaration of competing interest

The authors declare that they have no known competing financial interests or personal relationships that could have appeared to influence the work reported in this paper.

Acknowledgments

Financial support provided by the Dipartimento di Protezione Civile/Rete Laboratori Universitari Ingegneria Sismica e Strutturale, in Italian (DPC/ReLUIS) 2019-2021 Research Project, funded by the Civil Protection Department, allowed the authors to achieve the results reported in this paper.

List of symbols

a	Acceleration
A_c	Actual cross-sectional area of concrete of the column
$A_{c,req}$	Minimum required cross-sectional area of the column
a_g	Design ground acceleration on soil type A
A_s	Longitudinal rebar area
b_j	Base of the reinforced concrete joint
c	Cohesion
D	Damping ratio
D_s^*	Modified soil damping ratio
D_{s0}	Soil damping ratio at small strain
E_c	Concrete elastic modulus
E_s^*	Modified soil elastic modulus
E_{s0}	Soil elastic modulus at small strain
f	Frequency
F_0	Spectral amplification coefficient
f_1	First natural frequency
f_2	Second natural frequency
f_{ck}	Characteristic value of concrete cylinder compressive strength
f_{cm}	Mean value of concrete cylinder compressive strength
f_{ctm}	Mean value of concrete tensile strength
f_{max}	Maximum significant frequency of the dynamic input
f_{ym}	Mean value of steel yield stress
g	Acceleration of gravity
g_k	Characteristic values of the permanent loads
G_s^*	Modified soil shear modulus
G_{s0}	Soil shear modulus at small strain
H	Total thickness of the soil mesh
h	Soil layer thickness
h_c	Height of the reinforced concrete column
h_j	Height of the reinforced concrete joint
h_{max}	Maximum length of the mesh elements
I_0	Seismic intensity according to EMS
M	Bending moment
M_l	Local magnitude
M_s	Surface-wave magnitude
M_w	Moment magnitude
N	Design axial force of the column
n	Homogenisation coefficient for steel rebars
Ø	Diameter of the steel bars
q_k	Characteristic values of the variable loads
R_a	Amplification ratio
S	Soil factor
S_e	Spectral acceleration
S_S	Stratigraphic amplification factor

S_T	Topographic amplification factor
T	Period
t	Time
u	Horizontal displacement
V	Vertical component of the seismic motion
V_{max}	Maximum value of the shear force
V_{Rd}	Resistant shear force
V_s	Shear wave velocity
V_s^*	Modified shear wave velocity
$V_{s,eq}$	Weighted average value of the shear wave velocity up to the bedrock
$V_{s,av}$	Weighted average value of the modified shear wave velocities for the whole soil
w	Vertical displacement
z	Vertical depth
α	First Rayleigh damping factor
β	Second Rayleigh damping factor
φ'	Friction angle
γ_s	Soil unit weight
δ	Friction angle between the foundation and the soil
Δu	Soil-foundation relative horizontal displacement
Δw	Soil-foundation relative vertical displacement
ε_{c0}	Concrete strain at maximum strength
ε_{cu}	Concrete strain at crushing strength
θ	Curvature
ν_s	Soil Poisson's ratio
ρ_l	Ratio of the longitudinal rebar area A_s to $A_{c,req}$
ρ_s	Soil density
σ_c	Concrete allowable stress
σ_s	Steel allowable stress
φ'	Friction angle
ω_1	First natural angular frequency
ω_2	Second natural angular frequency

References

Abate, G., Caruso, C., Massimino, M.R., Maugeri, M., 2007. Validation of a new soil constitutive model for cyclic loading by FEM analysis. In: Ling, H.I., Callisto, L., Leshchinsky, D., Koseki, J. (Eds.), Soil Stress-Strain Behavior: Measurement, Modeling and Analysis. Solid Mechanics and its Applications, vol. 146. Springer, Dordrecht, The Netherland.

Abate, G., Caruso, C., Massimino, M.R., Maugeri, M., 2008. Evaluation of shallow foundation settlements by an elasto-plastic kinematic-isotropic hardening numerical model for granular soil. Geomechanics Geoengin. 3 (1), 27–40.

Abate, G., Massimino, M.R., Maugeri, M., Muir Wood, D., 2010. Numerical modelling of a shaking table test for soil-foundation-superstructure interaction by means of a soil constitutive model implemented in a FEM code. Geotech. Geol. Eng. 28 (1), 37–59.

Abate, G., Massimino, M.R., 2016. Dynamic soil-structure interaction by experimental and numerical modelling. Riv. Ital. Geotec. 50 (2), 44–70.

Abate, G., Massimino, M.R., Romano, S., 2016. Finite element analysis of DSSI effects for a building of strategic importance in Catania (Italy). Procedia Eng. 158, 374–379.

Abate, G., Grasso, S., Massimino, M.R., 2019. The role of shear wave velocity and non-linearity of soil in the seismic response of a coupled tunnel-soil-above ground building system. Geosciences 9 (11). https://doi.org/10.3390/geosciences9110473.

Abate, G., Bramante, S., Massimino, M.R., 2020. Innovative seismic microzonation maps of urban areas for the management of building heritage: a Catania case study. Geosciences 10 (12). https://doi.org/10.3390/geosciences10120480.

Aimar, M., Ciancimino, A., Foti, S., 2020. An assessment of the NTC18 stratigraphic seismic amplification factors. Riv. Ital. Geotec. 1, 5–21.

Alparone, S., D'Amico, S., Gambino, S., Maiolino, V., 2013. Buried active faults in the Zafferana Etnea territory (south-eastern flank of Mt. Etna): geometry and kinematics by earthquake relocation and focal mechanisms. Ann. Geophys. 56 (1). https://doi.org/10.4401/ag-5758.

Alparone, S., Maiolino, V., Mostaccio, A., Scaltrito, A., Ursino, A., Barberi, G., D'Amico, S., Di Grazia, G., Giampiccolo, E., Musumeci, C., Scarfi, L., Zuccarello, Z., 2015. Instrumental seismic catalogue of Mt. Etna earthquakes (Sicily, Italy): ten years (2000-2010) of instrumental recordings. Ann. Geophys.-Italy 58 (4). https://doi.org/10.4401/ag-6591.

Amendola, C., de Silva, F., Vratsikidis, A., Pitilakis, D., Anastasiadis, A., Silvestri, F., 2021. Foundation impedance functions from full-scale soil-structure interaction tests. Soil Dynam. Earthq. Eng. 141. https://doi.org/10.1016/j.soildyn.2020.106523.

Anastasiadis, A., Raptakis, D., Pitilakis, K., 2001. Thessaloniki's detailed microzoning: subsurface structure as basis for site response analysis. Pure Appl. Geophys. 158 (12), 2597–2633.

Andreotti, G., Famà, A., Lai, C., 2018. Hazard-dependent soil factors for site-specific elastic acceleration response spectra of Italian and European seismic building codes. Bull. Earthq. Eng. 16, 5769–5800.

Ansal, A., Kurtuluş, A., Tonuk, G., 2010. Seismic microzonation and earthquake damage scenarios for urban areas. Soil Dynam. Earthq. Eng. 30 (11), 1319–1328.

Ansal, A., Tonuk, G., Kurtuluş, A., 2019. Microzonation with respect to ground shaking intensity. In: Silvestri, F., Moraci, N. (Eds.), Earthquake Geotechnical Engineering for Protection and Development of Environment and Constructions - Proceedings of the 7th International Conference on Earthquake Geotechnical Engineering (ICEGE 2019). Rome, Italy, pp. 410–425.

Azzaro, R., 2004. Seismicity and active tectonics in the Etna region: constraints for a seismotectonic model. In: Bonaccorso, A., Calvari, S., Coltelli, M., Del Negro, C., Falsaperla, S. (Eds.), Mt. Etna: Volcano Laboratory, Geophysical Monograph, vol. 143. American Geophysical Union, Washington, DC, USA, pp. 205–220.

Azzaro, R., Barbano, M.S., D'Amico, S., Tuvè, T., Albarello, D., D'Amico, V., 2008. First studies of probabilistic seismic hazard assessment in the volcanic region of Mt. Etna (Southern Italy) by means of macroseismic intensities. Boll. di Geofis. Teor. ed Appl. 49 (1), 77–91.

Azzaro, R., D'Amico, S., Tuvè, T., 2011. Estimating the magnitude of historical earthquakes from macroseismic intensity data: new relationships for the volcanic region of MountEtna (Italy). Seismol Res. Lett. 82 (4), 520–531.

Azzaro, R., Branca, S., Gwinner, K., Coltelli, M., 2012. The volcano-tectonic map of Etna volcano, 1:100.000 scale: an integrated approach based on a morphotectonic analysis from high-resolution DEM constrained by geologic, active faulting and seismotectonic data. Ital. J. Geosci. 131 (1), 153–170.

Azzaro, R., D'Amico, S., Peruzza, L., Tuvè, T., 2013. Probabilistic seismic hazard at Mt. Etna (Italy): the contribution of local fault activity in mid-term assessment. J. Volcanol. Geoth. Res. 251, 158–169.

Azzaro, R., Bonforte, A., Branca, S., Guglielmino, F., 2014. Geometry and kinematics of the fault systems controlling the unstable flank of Etna volcano (Sicily). J. Volcanol. Geoth. Res. 251, 5–15.

Bardet, J.P., Ichii, K., Lin, C.H., 2000. EERA -A Computer Program for Equivalent-Linear Earthquake Site Response Analyses of Layered Soil Deposits. University of Southern California, USA.

Bathe, K.J., 1999. Nonlinear finite element analysis and ADINA. In: Bathe, K.J. (Ed.), Proceeedings of the 12th ADINA Conference on Computers and Structures. Elsevier Science, Oxford, UK.

Bielak, J., 1971. Earthquake Response of Building-Foundation Systems. PhD Thesis. California Institute of Technology, USA.

Chaudhuri, C.H., Chanda, D., Saha, R., Haldar, S., 2020. Three-dimensional numerical analysis on seismic behavior of soil-piled raft-structure system. Structures 28, 905–922.

Chopra, A.K., 1995. Dynamics of Structures: Theory and Applications to Earthquake Engineering, fifth ed. Pearson College, Englewood Cliffs, New Jersey, USA.

Ciancimino, A., Foti, S., Lanzo, G., 2018. Stochastic analysis of seismic ground response for site classification methods verification. Soil Dynam. Earthq. Eng. 11, 169–183.

Civico, R., Pucci, S., Nappi, R., Azzaro, R., Villani, F., Pantosti, D., Cinti, F.R., Pizzimenti, L., Branca, S., Brunori, C.A., Caciagli, M., Cantarero, M., Cucci, L., D'Amico, S., De Beni, E., De Martini, P.M., Mariucci, M.T., Montone, P., Nave, R., Ricci, T., Sapia, V., Smedile, A., Tarabusi, G., Vallone, R., Venuti, A., 2019. Surface ruptures following the 26 December 2018, Mw 4.9, Mt. Etna earthquake, Sicily (Italy). J. Maps 15 (2), 831–837.

CMTE Working Group, 2008. Catalogo Macrosismico dei Terremoti Etnei, 1832–2008. Istituto Nazionale di Geofisica e Vulcanologia, Catania. http://www.ct.ingv.it/ufs/macro/. (Accessed 28 December 2021).

DM, 1976. Norme tecniche per la esecuzione delle opere in cemento armato normale e precompresso e per le strutture metalliche. Gazzetta Ufficiale Della Repubblica Italiana Suppl. Ord. 14/08/1976 (in Italian).

Elwardany, H., Seleemah, A., Jankowski, R., El-khoriby, S., 2019. Influence of soil–structure interaction on seismic pounding between steel frame buildings considering the effect of infill panels. Bull. Earthq. Eng. 17, 6165–6202.

EN 1998-1, 2004. Eurocode 8: Design of Structures for Earthquake Resistance - Part 1: General Rules, Seismic Actions and Rules for Buildings. European Committee for Standardization, Brussels, Belgium.

EN 1998-3, 2004. Eurocode 8: Design of Structures for Earthquake Resistance - Part 3: Assessment and Retrofitting of Buildings. European Committee for Standardization, Brussels, Belgium.

EN 1998-5, 2004. Eurocode 8: Design of Structures for Earthquake Resistance - Part 5: Foundations, Retaining Structures and Geotechnical Aspects. European Committee for Standardization, Brussels, Belgium.

FEMA P-2082-1, 2009. NEHRP Recommended Seismic Provisions for New Buildings and Other Structures. Building Seismic Safety Council of the National Institute of Building Sciences for the Federal Emergency Management Agency, Washington, DC, USA.

Ferraro, A., Grasso, S., Massimino, M.R., Maugeri, M., 2015. Influence of geotechnical parameters and numerical modelling on local seismic response analysis. In: Winter, M.G., Smith, D.M., Eldred, P.J.L., Toll, D.G. (Eds.), Proceedings of the 16th European Conference on Soil Mechanics and Geotechnical Engineering (ECSMGE 2015), pp. 2183–2188.

Ferraro, A., Grasso, S., Massimino, M.R., 2018. Site effects evaluation in Catania (Italy) by means of 1-D numerical analysis. Ann. Geophys. 61 (2). https://doi.org/10.4401/ag-7708.
Google Earth, 2021. Map Showing Location of Zafferana Etnea and the Building under Study, Google Earth. https://www.google.com/intl/it/earth/. (Accessed 28 December 2021).
Hashash, Y.M.A., Musgrove, M.I., Harmon, J.A., Ilhan, O., Xing, G., Numanoglu, O., Groholski, D.R., Phillips, C.A., Park, D., 2020. DEEPSOIL 7.0, User Manual. Board of Trustees of University of Illinois at Urbana-Champaign, Urbana, IL.
Jarernprasert, S., Bazan-Zurita, E., Bielak, J., 2013. Seismic soil-structure interaction response of inelastic structures. Soil Dynam. Earthq. Eng. 47, 132–143.
Karatzetzou, A., Pitilakis, D., 2017. Modification of dynamic foundation response due to soil-structure interaction. J. Earthq. Eng. 22 (5), 861–880.
Kausel, E., 2010. Early history of soil-structure interaction. Soil Dynam. Earthq. Eng. 30 (9), 882-832.
Kottke, A., Rathje, E., 2008. Technical Manual for Strata PEER Report 2008/10. University of California, USA.
Kwok, A.L., Stewart, J.P., Hashash, Y.M., Matasovic, N., Pyre, R., Wang, Z., Yang, Z., 2007. Use of exact solutions of wave propagation problems to guide implementation of nonlinear seismic ground response analysis procedures. J. Geotech. Eng. 133 (11), 1385–1398.
Lanzo, G., Silvestri, F., 1999. Risposta Sismica Locale, first ed. Helvelius, Napoli, Italy.
Lanzo, G., Silvestri, F., Costanzo, A., d'Onofrio, A., Martelli, L., Pagliaroli, A., Sica, S., Simonelli, A., 2011. Site response studies and seismic microzoning in the Middle Aterno valley (L'aquila, central Italy). Bull. Earthq. Eng. 9 (5), 1417–1442.
Luco, J.E., 1980. Linear Soil-Structure Interaction. Lawrence Livermore National Laboratory. UCRL-15272.
Luzi, L., Pacor, F., Puglia, R., 2019. Italian Accelerometric Archive v3.0. Istituto Nazionale di Geofisica e Vulcanologia, Dipartimento della Protezione Civile Nazionale. https://doi.org/10.13127/itaca.3.0.
Lysmer, J., Kuhlemeyer, R.L., 1969. Finite dynamic model for infinite media. J. Eng. Mech. 95 (4), 859–877.
Lysmer, J., Ostadan, F., Chin, C., 1999. Computer Program SASSI2000 – a System for Analysis of Soil-Structure Interaction. University of California, Berkeley, California, USA.
Mander, J.B., Priestley, M.J., Park, R., 1988. Theoretical stress-strain model for confined concrete. J. Struct. Eng. 114 (8). https://doi.org/10.1061/(ASCE)0733-9445(1988)114:8(1804).
Masi, A., Digrisolo, A., Santarsiero, G., 2014. Concrete strength variability in Italian RC buildings: analysis of a large database of core tests. Appl. Mech. Mater. 597, 283–290.
Massimino, M.R., Biondi, G., 2015. Some experimental evidences on dynamic soil-structure interaction. In: Proceedia, E.C.C.O.M.A.S. (Ed.), Proceedings of the 5th International Conference on Computational Methods in Structural Dynamics and Earthquake Engineering Methods in Structural Dynamics and Earthquake Engineering, pp. 2761–2774.
Massimino, M.R., Abate, G., Grasso, S., Pitilakis, D., 2019a. Some aspects of DSSI in the dynamic response of fully-coupled soil-structure systems. Riv. Ital. Geotec. 1, 44–70.
Massimino, M.R., Abate, G., Corsico, S., Louarn, R., 2019b. Comparison between two approaches for nonlinear FEM modelling of the seismic behaviour of a coupled soil–structure system. Geotech. Geol. Eng. 37 (3), 1957–1975.
Maugeri, M., Abate, G., Massimino, M.R., 2012. Soil-structure interaction for seismic improvement of Noto Cathedral (Italy). Geotech. Geol. Earthq. Eng. 16, 217–239.
Mazzoni, S., McKenna, F., Scott, M.H., Fenves, G.L., 2006. OpenSees command language manual. Pac. Earthq. Eng. Res. (PEER) Center 264, 137–158.
Mercado, J.A., Arboleda-Monsalve, L.G., Mackie, K.R., 2021. Nonlinear inelastic-degrading structural modeling approach to assess the seismic soil-structure interaction response of tall buildings. J. Geotech. Geoenviron. Eng. 147 (10). https://doi.org/10.1061/(ASCE)GT.1943-5606.0002628.
Muir Wood, D., 2004. Geotechnical Modelling. E&FN Spon, London, UK.
Mylonakis, G., Gazetas, G., 2000. Seismic soil-structure interaction: beneficial or detrimental? J. Earthq. Eng. 4 (3), 277–301.
Mylonakis, G., Nikolaou, S., Gazetas, G., 2006. Footings under seismic loading: analysis and design issues with emphasis on bridge foundations. Soil Dynam. Earthq. Eng. 26, 824–853.
NTC, 2018. Norme Tecniche per le Costruzioni. Gazzetta Ufficiale Della Repubblica Italiana Suppl. Ord. 20/02/2018 (in Italian).
Özcebe, A.G., Giretti, D., Bozzoni, F., Fioravante, V., Lai, C.G., 2021. Centrifuge and numerical modelling of earthquake induced soil liquefaction under free field conditions and by considering soil–structure interaction. Bull. Earthq. Eng. 19, 47–75.
Pagliaroli, A., Pergalani, F., Ciancimino, A., Chiaradonna, A., Compagnoni, M., de Silva, F., Foti, S., Giallini, G., Lanzo, F., Lombardi, F., Luzi, F., Macerola, L., Nocetini, M., Pizzi, A., Tallini, M., Teramo, C., 2020. Site response analyses for complex geological and morphological conditions: relevant case-histories from 3rd level seismic microzonation in Central Italy. Bull. Earthq. Eng. 18 (12), 5741–5777.
Paolucci, R., Shirato, M., Yilmaz, M.T., 2008. Seismic behaviour of shallow foundations: shaking table experiment vs. numerical modelling. Earthq. Eng. Struct. Dynam. 37 (4), 577–595.
Paolucci, R., Aimar, M., Ciancimino, A., Dotti, M., Foti, S., Lanzano, G., Mattevi, P., Pacor, F., Vanini, M., 2021. Checking the site categorization criteria and amplification factors of the 2021 draft of Eurocode 8 Part 1–1. Bull. Earthq. Eng. 19, 4199–4234.
Patanè, D., Cocina, O., Falsaperla, S., Privitera, E., Spampinato, S., 2004. Mt. Etna Volcano: a seismological framework. In: Bonaccorso, A., Calvari, S., Coltelli, M., Del Negro, C., Falsaperla, S. (Eds.), Mt. Etna: Volcano Laboratory, Geophysical Monograph, vol. 143. American Geophysical Union, Washington, DC, USA, pp. 205–220.
Pistolas, G.A., Pitilakis, K., Anastasiadis, A., 2020. A numerical investigation on the seismic isolation potential of rubber/soil mixtures. Earthq. Eng. Eng. Vib. 19 (3), 683–704.
Pitilakis, D., Dietz, M., Miur Wood, D., Clouteau, D., Modaressi, A., 2008. Numerical simulation of dynamic soil-structure interaction in shaking table testing. Soil Dynam. Earthq. Eng. 28 (6), 453–467.
Pitilakis, K., Riga, E., Anastasiadis, A., 2012. Design spectra and amplification factors for Eurocode 8. Bull. Earthq. Eng. 10 (5), 1377–1400.
Pitilakis, K., Riga, E., Anastasiadis, A., Fotopoulou, S., Karafagka, S., 2019. Towards the revision of EC8: proposal for an alternative site classification scheme and associated intensity dependent spectral amplification factors. Soil Dynam. Earthq. Eng. 126. https://doi.org/10.1016/j.soildyn.2018.03.030.
Pitilakis, D., Anastasiadis, A., Vratsikidis, A., Kapouniaris, A., Massimino, M.R., Abate, G., Corsico, S., 2021. Large-scale field testing of geotechnical seismic isolation of structures using gravel-rubber mixtures. Earthq. Eng. Struct. Dynam. 50 (10), 2712–2731.
QUEST-WG, 2019. Il terremoto etneo del 26 dicembre 2018, Mw4.9: rilievo degli effetti macrosismici. Rapporto INGV No.1 del 06/02/2019 1–9. https://doi.org/10.5281/zenodo.2558168 (in Italian).
Rovithis, E., Kirtas, E., Bliziotis, D., Maltezos, E., Pitilakis, D., Makra, K., Savvaidis, A., Karakostas, C., Lekidis, V., 2017. A LiDAR-aided urban-scale assessment of soil-structure interaction effects: the case of Kalochori residential area (N. Greece). Bull. Earthq. Eng. 15, 4821–4850.
Simeone, A., 2018. Evoluzione delle caratteristiche delle armature del c.a. dal 1960 ai giorni nostri. MSc Thesis, Politecnico Di Torino, Turin, Italy (in Italian).
Tropeano, G., Soccodato, F.M., Silvestri, F., 2018. Re-evaluation of code-specified stratigraphic amplification factors based on Italian experimental records and numerical seismic response analyses. Soil Dynam. Earthq. Eng. 110, 262–275.
Veletsos, A.S., Meek, J.W., 1974. Dynamic behaviour of building-foundation systems. Earthq. Eng. Struct. Dynam. 3 (2), 121–138.
Wang, Q., Wang, J.T., Jin, F., Chi, F.D., Zhang, C.H., 2011. Real-time dynamic hybrid testing for soil–structure interaction analysis. Soil Dynam. Earthq. Eng. 31 (12), 1690–1702.
Wolf, J.P., 1985. Dynamic Soil–Structure Interaction. Prentice-Hall, Englewood Cliffs, NJ, USA.

Angela Fiamingo is a PhD student from the Department of Civil Engineering and Architecture, University of Catania, Italy. In 2020, she obtained her MSc degree in Structural and Geotechnical Civil Engineering from the University of Catania, Italy, with full marks and honour. Her current research interests cover the study of the Dynamic Soil-Structure Interaction (DSSI) and the Geotechnical Seismic Isolation (GSI) systems, using soil and rubber grains, manufactured from scrap tyres, disposal of which has become a severe environmental problem worldwide.